Astronomy & Astrophysics manuscript no. 3470
February 2, 2008

The pulsation modes of the pre-white dwarf PG 1159-035

J. E. S. Costa[1], S. O. Kepler[1], D. E. Winget[2], M. S. O'Brien[47], S. D. Kawaler[4], A. F. M. Costa[1], O. Giovannini[1,5], A. Kanaan[6], A. S. Mukadam[42], F. Mullally[2], A. Nitta[3], J. L. Provençal[8], H. Shipman[8], M. A. Wood[9], T. J. Ahrens[9], A. Grauer[10], M. Kilic[41], P. A. Bradley[11], K. Sekiguchi[12], R. Crowe[13], X. J. Jiang[14], D. Sullivan[15], T. Sullivan[15], R. Rosen[15], J. C. Clemens[16], R. Janulis[17], D. O'Donoghue[18], W. Ogloza[19], A. Baran[19], R. Silvotti[20], S. Marinoni,[21], G. Vauclair[22], N. Dolez[22], M. Chevreton[23], S. Dreizler[24,25], S. Schuh[24,25], J. Deetjen[24], T. Nagel[24], J.-E. Solheim[26,27], J. M. Gonzalez Perez[26,28], A. Ulla[29], Martin Barstow[30], M. Burleigh[30], S. Good[30], T.S. Metcalfe[31], S.-L. Kim[32], H. Lee[32], A. Sergeev[33], M.C. Akan[34], Ö. Çakırlı[34], M. Paparo[35], G. Viraghalmy[35], B. N. Ashoka[36], G. Handler[37], Özlem Hürkal[38], F. Johannessen[26], S. J. Kleinman[3], R. Kalytis[17], J. Krzesinski[19], E. Klumpe[39], J. Larrison[39], T. Lawrence[4], E. Meištas[17], P. Martinez[18], R. E. Nather[2], J.-N. Fu[48], E. Pakštienė[17], R. Rosen[26], E. Romero-Colmenero[18], R. Riddle[44], S. Seetha[37], N. M. Silvestri[42], M. Vučković[4,43], B. Warner[18], S. Zola[40], L. G. Althaus[45,46], A. H. Córsico[45,46], and M. H. Montgomery[2]

(Affiliations can be found after the references)

2007 Aug 28 Received —; accepted 2007 Oct 31

ABSTRACT

Context. PG 1159-035, a pre-white dwarf with $T_{\rm eff} \simeq 140\,000$ K, is the prototype of both two classes: the PG 1159 spectroscopic class and the DOV pulsating class. Previous studies of PG 1159-035 photometric data obtained with the Whole Earth Telescope (WET) showed a rich frequency spectrum allowing the identification of 122 pulsation modes. Analyzing the periods of pulsation, it is possible to measure the stellar mass, the rotational period and the inclination of the rotation axis, to estimate an upper limit for the magnetic field, and even to obtain information about the inner stratification of the star.

Aims. We have three principal aims: to increase the number of detected and identified pulsation modes in PG 1159-035, study trapping of the star's pulsation modes, and to improve or constrain the determination of stellar parameters.

Methods. We used all available WET photometric data from 1983, 1985, 1989, 1993 and 2002 to identify the pulsation periods.

Results. We identified 76 additional pulsation modes, increasing to 198 the number of known pulsation modes in PG 1159-035, the largest number of modes detected in any star besides the Sun. From the period spacing we estimated a mass $M/M_{\odot} = 0.59 \pm 0.02$ for PG 1159-035, with the uncertainty dominated by the models, not the observation. Deviations in the regular period spacing suggest that some of the pulsation modes are trapped, even though the star is a pre-white dwarf and the gravitational settling is ongoing. The position of the transition zone that causes the mode trapping was calculated at $r_c/R_{\star} = 0.83 \pm 0.05$. From the multiplet splitting, we calculated the rotational period $P_{\rm rot} = 1.3920 \pm 0.0008$ days and an upper limit for the magnetic field, $B < 2000$ G. The total power of the pulsation modes at the stellar surface changed less than 30% for $\ell = 1$ modes and less than 50% for $\ell = 2$ modes. We find no evidence of linear combinations between the 198 pulsation mode frequencies. PG 1159-035 models have not significative convection zones, supporting the hypothesis that nonlinearity arises in the convection zones in cooler pulsating white dwarf stars.

Key words. stars: oscillations — stars: individual: PG 1159-035 — stars: rotation

1. Introduction

The star PG 1159-035 was identified by R. F. Green in 1977 in a survey for objects with ultraviolet excess, known as the Palomar-Green Survey (Green et al. 1986). The presence of lines of He II in the PG 1159-035 spectrum suggested a high superficial temperate (McGraw et al. 1979). The analysis of the far ultraviolet flux distribution — from ∼ 1200 Å to the Lyman limit at 912 Å — obtained with the *Voyager 2* ultraviolet spectrophotometer indicated an effective temperature above 100 000 K (Wegner et al. 1982). Later analysis with the *IUE* and *EXOSAT* show that PG 1159-035 is one of the hottest stars known (Sion et al. 1985, Barstow et al. 1986); the current estimated temperature for PG 1159-035 is 140 000±5 000 K (Werner et al. 1991, Dreizler et al. 1998 and Jahn et al. 2007) and $\log g(cgs) = 7.0 \pm 0.5$ (Werner et al. 1991), placing it in the class of the pre-white dwarf stars.

McGraw et al. (1979) discovered that PG 1159-035 is a variable star and identified at least two pulsation periods. The Fourier transform of more extensive light curves obtained in the following years, between 1979-1985, allowed the detection of eight pulsation modes (Winget et al. 1985); the highest amplitude mode has a period of 516 *s*.

A long light curve is necessary to resolve two nearby frequencies in the Fourier transform (FT) of a multiperiodic pulsating star. The Fourier transform resolution is roughly proportional to the inverse of the light curve length. For instance, if the difference between two frequencies is equal to 100 μHz, just three hours of photometric data are needed to resolve them, but, more than 10 days are needed if the difference between them is of 1 μHz. On other hand, the presence of gaps in the light curve introduces in the FT an intricate structure of side-lobes, which may hinder the detection and identification of real pulsation frequencies.

Send offprint requests to: costajes@gmail.com

With the establishment of the WET (*Whole Earth Telescope*) in 1988 (Nather et al. 1990), PG 1159-035 was observed for about 12 days with an effective coverage around 60%, resulting in a quasi-continuous 228 hours of photometric data. The high-resolution Fourier transform of the light curve allowed the detection and identification of 122 peaks (Winget et al. 1991).

In white dwarf and pre-white dwarf stars, gravity plays the role of the restoring force in the oscillations. Any radial displacement of mass suffers the action of the gravitational force causing the displaced portion of mass to be scattered inwards and sideways. This type of nonradial pulsation modes are called *g-modes*.

General nonradial pulsations are characterized by three integer numbers: k, ℓ, m. The number k is called *radial index* and is related with the number of *nodes* in the radial direction of the star. The number ℓ is called *index of the spherical harmonic* (or *degree of the pulsation mode*). For nonradial modes, $\ell > 0$, while a radial pulsation has $\ell = 0$. In white dwarf stars the pulsations are dominated by temperature variations (Robinson, Kepler, and Nather 1982). The index ℓ is related with the total number of hotter and colder zones relative to the mean effective temperature on the stellar surface. Finally, the number m is a number between $-\ell$ and $+\ell$ and is called the *azimuthal index*. The degeneracy of modes with different m is broken when the spherical symmetry is broken, for example, by rotation of the star, or the presence of magnetic fields. The absolute value of the azimuthal index, $|m|$, is related with the way the cold zones and hot zones are arranged on the stellar surface. The sign of the index m indicates the direction of the temporal pulsation propagation. We adopted the convention used by Winget et al. (1991): m is positive if the pulsation and the rotation have the same direction and negative if they have opposite directions.

The PG 1159-035 Fourier transform published in 1991 also revealed the presence of triplets and multiplets, caused by *rotational splitting*, allowing the determination of the rotational period of the star ($P_{rot} = 1.38$ days). Stellar rotation causes the g-modes with $m \neq 0$ to appears in the FTs as frequencies slightly higher ($m > 0$) or lower ($m < 0$) than the frequency of the $m = 0$ mode, depending on whether the pulsation is travelling in the same direction of the rotation of the star (higher frequency) or in opposite direction (lower frequency). Slow rotation splits a mode in a multiplet of $2(\ell + 1)$ peaks. For $\ell = 1$ modes, the multiplets have three peaks (triplets) and for $\ell = 2$ modes they have five peaks (quintuplets). But not necessarily all components are seen in the FTs, because some of them might be excited with amplitudes bellow the detection limit. Besides stellar rotation, a weak magnetic field can also break the degeneracy and cause an observable splitting of the pulsation modes into $(\ell + 1)$ components in first order. However, no notable magnetic splitting has been observed in PG 1159-035 (Winget et al. 1991).

The immediate goal of this work was to detect and identify a larger number of pulsating modes in PG 1159-035 from the analysis and comparison of the FTs of photometric data obtained in different years. A consequence is the improvement in the determination of the spacing between the periods of the pulsation modes used in the calculation of the stellar mass and in the determination of the inner stratification of the star. The analysis of the splitting in frequency in the multiplets of the combined data allows the calculation of the rotation period with higher accuracy and a better estimate of a upper limit for the strength of the star's magnetic field. We are also interested in the search for possible linear combination of frequencies, as an indication of nonlinear behavior.

This paper is organized as follow: in next Section we present some basic background in pulsation theory. In §3 and §4 we discuss the observational data and the data reduction process used in this work. In §5 we discuss the detection of pulsation modes from the PG 1159-035 FTs. Then, in §6, we present the calculation of the period spacing for the detected pulsation modes. The mode identification, i.e., the determination of the numbers k, ℓ and m of the detected pulsation modes is discussed in §7 and in §8 §9 we calculate the rotational and the magnetic splittings and the rotation period of the star. An estimate of the inclination angle of the rotational axis of the star is done in §10 and in §11 we use the splitting to obtain an upper limit for the PG 1159-035 magnetic field. In §12 we present the estimate of the mass of PG 1159-035 from the period spacing in comparison with the masses calculated from spectroscopic models. The analysis of a possible trapping of pulsation modes in PG 1159-035 is presented in §13 and in §14 we use the results to calculate the position of a possible trapping zone inside the star. In §15 we comment on the absence of linear combination of frequencies in PG 1159-035 and in §16 on the energy conservation of the pulsation modes in the star surface. Finally, in §17 we summarize our main results.

2. Some Background

The periods of g-modes for a given ℓ must increase monotonically with the number of radial nodes, k. This occurs because the restoring force is proportional to the displaced mass, which is smaller when the number of radial nodes, k, is larger. For white dwarfs and pre-white dwarfs stars, a weaker restoring force implies in a longer period. One of the known methods to calculate the oscillation periods inside a resonant cavity is the WKB (Wentzel-Kramers-Brillouin) approximation, well know in Quantum Mechanics [see, for instance, Sakurai (1994)]. In the case of pulsating stars, this approximation is based on the hypothesis that the wavelength of the radial wave is much smaller than the length scales in which the relevant physical variables (density, for example) are changing inside the star. This is approximately true for g-modes with large values of k ($k \gg \ell$). In this asymptotic limit, e.g. Kawaler et al. (1985) the WKB result approaches a simple expression:

$$P_{\ell,k} \simeq \frac{P_o}{\sqrt{\ell(\ell+1)}}\, k + \epsilon \qquad (1)$$

where, $P_{\ell k}$ is the period with index ℓ and k and P_o and ϵ are constants (in seconds). The mean spacing between two consecutive periods ($P_{\ell,k+1} - P_{\ell,k}$) of same ℓ is:

$$\Delta P_\ell \simeq \frac{P_o}{\sqrt{\ell(\ell+1)}} \qquad (2)$$

The constant P_o in Eq.1 strongly depends on the stellar mass (Kawaler and Bradley 1994) and, therefore, the determination of ΔP_ℓ allows us to measure the mass of the star. On the other hand, the internal stratification of the star causes the differences $P_{\ell,k+1} - P_{\ell,k}$ to have small deviations relative to the mean spacing, ΔP_ℓ. The analysis of these deviations can give us relevant information about the internal structure of the star.

3. The Observational Data

PG 1159-035 has been observed with time series photometry at McDonald Observatory since 1979, soon after being identified

Table 1. Observational campaigns of PG 1159-035 between 1979-2002.

Year	Number of datum	Length (days)	Hours of photometry (h)	Effective coverage	Overlapping rate	Spectral resolution (μHz)
1979	523	0.1	2.9	100.0%	—	95.0
1980	1 294	5.1	7.2	5.9%	—	2.3
1983	11 758	96.0	64.5	2.8%	—	0.2
1984	2 658	1.3	14.8	47.4%	—	5.0
1985	4 380	64.6	48.1	3.0%	0.1%	0.2
1989	82 471	12.1	228.8	65.4%	13.4%	1.0
1990	11 690	7.7	16.2	8.8%	—	1.5
1993	248 162	16.9	345.2	64.3%	20.8%	0.7
2000	14 794	10.3	24.5	9.2%	0.7%	1.1
2002	33 770	14.8	116.5	27.7%	5.1%	0.8

as a pulsating star by McGraw et al. (1979). In 1983 the star was observed several times during three months, revealing the presence of at least eight pulsation frequencies. New observations were obtained in 1984 and 1985 (Winget et al. 1985), confirming the persistence of the previously detected pulsation modes. Campaigns of quasi-continuous observations were carried out with WET in 1989, 1990, 1993, 2000 and 2002; however, in 1990, 2000 and 2002 PG 1159-035 was observed as a secondary target.

Details about the observational campaigns are given in Table 1. The *overlapping rate*, in column six, is the fraction of time in which two telescopes carry out simultaneous observations of the star causing an overlap of photometric measurements in the total light curve. The *spectral resolution*, in the last column, is the approximate mean width of the frequency peaks (in μHz) in the FT of the total light curve of each yearly data set. Logs and additional information about the observational campaigns are presented in Winget et al. (1985), Winget et al. (1991), Bruvold (1993) and Costa et al. (2003).

4. Data Reduction

The reduction of the photometric data was based on the process described by Nather et al. (1990) and Kepler et al. (1995), but with some additional care in the atmospheric correction.

Most of the observations were obtained with three channel photometers. While one of the channels is used to observe the target star, another channel observes a non-variable star used as comparison star, and measurement of the adjacent sky are taken with the third channel. After discarding bad points in the light curve of the three channels, the measurements are calibrated and the sky level is subtracted from the light curves of the two stars (target and comparison). To correct by atmospheric extinction to first order, the light curve of the target star is divided, point-by-point, by the light curve of the comparison star.

The most critical step in the data reduction is the atmospheric correction. During the night, the sky transparency changes on different timescales, affecting the light curves of the two stars. The division of the light curve of the target star by the light curve of the comparison star does not completely eliminate the effect of atmospheric extinction in the resulting light curve, because the atmospheric extinction effect is dependent of the star color and in most of the cases the two stars do not have the same color (PG 1159-035 is blue). This implies that some residual signal due to the atmospheric extinction remains in the resulting light curve, appearing in the FTs of the individual nights as one or more peaks of low frequency ($f < 300\,\mu$Hz) and relative high amplitude, as shown in the left graph in Fig. 1 (see also Breger and Handler 1993).

We performed numerical simulations to study the effect of signals with low frequency and high amplitude (LFHA) on the determination of the parameters of the pulsation modes (frequency, amplitude and phase). Our results show that the LFHA can introduce *significant* errors in the determinations of the frequencies, amplitudes and phases of the pulsation modes. For pulsating stars, as PG 1159-035, with many pulsation modes with low amplitudes ($A < 1\,mma$), this interference can represent a serious problem.

To minimize this effect, we fitted a polynomial of 4$^{\rm th}$ order to the light curve of each individual night, but even so, residual frequencies with considerable amplitude persisted in the residual light curve. To eliminate them, we used a *high-pass filter*, an algorithm that detects and eliminates signals with high amplitudes and frequencies lower than 300 μHz, as illustrated in Fig. 1. Note that the limit of 300 μHz is far less than our frequency range of interest, 1000 − 3000 μHz, where we see the pulsation modes. We note that *all* signals with frequencies lower than 300 μHz, even if they are present in the star, are eliminated.

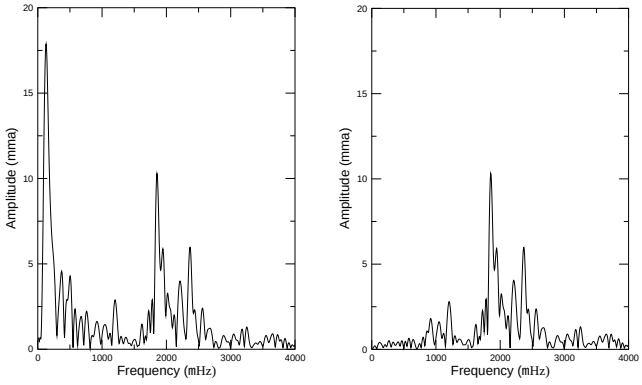

Fig. 1. Left: Fourier transform of the light curve of an individual night with peaks of low frequency and high amplitude. Right: Fourier transform of the same light curve after the use of a high-pass filter.

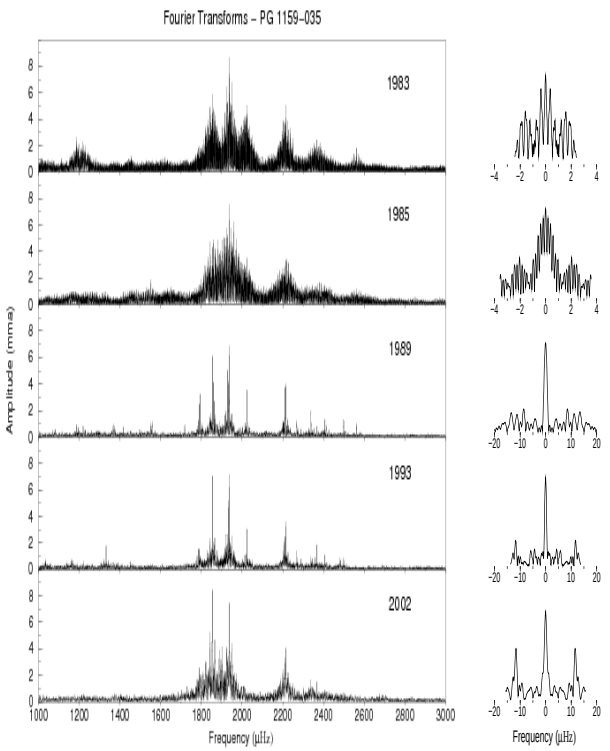

Fig. 2. Periodograms of PG 1159-035 of the years of 1983, 1985, 1989, 1993 and 2002. The respective spectral windows are shown on the right.

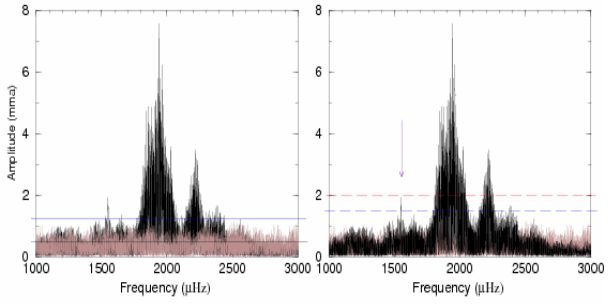

Fig. 3. Periodogram of the 1985 data set of PG 1159-035 (dark) and the FT of the same data set randomized (light). Note that the randomization destroys all signals. The horizontal solid lines in the *left* graph show the levels: $\bar{A}$ (upper) and $\bar{A}_m$ (lower); while the graph *right* show the detection limits of $A_1 = 4\bar{A}$ (upper) and A_0 (lower). The arrow shows a peak that is not detected when the limit of A_1 is used.

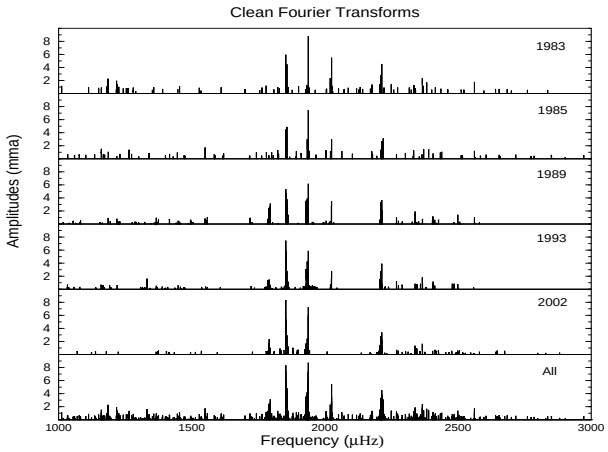

Fig. 4. The clean Fourier transform for each annual light curve of PG 1159-035. The bottom graph is a merge of the clean Fourier transforms of all years.

5. Detection of Pulsating Periods

Figure 2 shows the FTs for each one of the annual light curves of PG 1159-035 for the frequency range of interest (1000 − 3000 μHz). Frequency is in μHz and amplitude is in units of *mma* (milli-modulation amplitude). The respective spectral windows are on the right side, with the same scale in amplitude, but different scale in frequency.

To find pulsation frequencies, we used an iterative approach: (0) starting with an empty list of candidate frequencies and with the FT of the original light curve; (1) identify, inside the range of interest in the FT, the peaks with amplitudes above the detection limit (taking care to discard aliases). If there is no peak above the detection limit, the algorithm stops. (2) Put the detected frequencies in the list of candidate frequencies, and (3) using a nonlinear method, fit sinusoidal curves using *all* frequencies from the list based on the original light curve. The fitting refines the values of the initial frequencies and calculates their amplitudes and phases. (4) The fitted sinusoidals are subtracted from the original light curve and the FT of the residual light curve is calculated. Then, the algorithm returns to the step (1) to search for other possible pulsation frequencies.

Usually, the detection limit is based on the local average amplitude of the peaks in the FT, $\bar{A}$. Kepler (1993) and Schwarzenberg-Czerny (1991, 1999), following Scargle (1982), demonstrated that non-equally spaced data sets of multiperiodic light curves do not follow a normal noise distribution, because the residuals are correlated. They conclude that the probability of a peak in the FT above $4\bar{A}$ has a 1/1000 chance of being due to noise (therefore, not a real signal) for a large frequency range of interest (see also Breger and Handler 1993 and Kuschnig et al. 1997 for similar estimates).

The comparison of the FTs of the light curves of the different years shows that a mode can appear with an amplitude above the limit of $4\bar{A}$ in one FT and have a amplitude below this limit in the FT of another year. To detect a larger number of pulsation modes we used a lower detection limit. The presence of a same peak in different FTs reinforces the probability of it being a real pulsation mode.

A lower detection limit was empirically estimated from the following Monte Carlo simulation: (1) the light curve is randomized and (2) its FT is calculated for the frequency range of interest. (3) The highest peak in the FT, $A_{\max}$ is found and computed. The sequence above is repeated 1000 times and (4) the average amplitude for the higher peak, $\langle A_{\max}\rangle$ and its standard deviation, σ are calculated. Then, (5) the detection limit is defined as $A_{\rm detect} = \langle A_{\max}\rangle + 3.5\sigma$. In all our cases, the factor 3.5σ is $\sim 20\%$ of $\langle A_{\max}\rangle$, therefore, $A_{\rm detect} = 1.2\,\langle A_{\max}\rangle$.

This way to define the detection limit doesn't take into account that the real noise is not white, *but* the calculation uses the same temporal sampling of the original light curve and the same frequency range used in the frequency analysis.

We classified the peaks of each FT into the six probability levels listed in Table 2. Initially, we selected all peaks with probability levels 1-4. Of course, with the inclusion of peaks with lower probability levels the chance of including false pulsation

Table 2. Confidence levels of the found peaks.

Level	Description
1	Peak with amplitude $A \geq 4\bar{A}$ and appearing in one or more of the FTs
2	Peak with amplitude $4\bar{A} > A \geq A_{\rm detect}$ and appearing in two or more FTs
3	Peak with amplitude $4\bar{A} > A \geq A_{\rm detect}$, but appearing only in one of the FTs
4	Peak with amplitude $A < A_{\rm detect}$, but appearing in two or more FTs with an amplitude greater than the nearest peaks.
5	Peak with amplitude $A < A_{\rm detect}$, appearing in only one of the FTs with an amplitude greater than the nearest peaks.
6	Peak with amplitude $A < A_{\rm detect}$ in all FTs, with amplitudes not higher than the amplitude of the nearest peaks.

frequencies increases, but we hope to be able to discard the major part of them analyzing their places into multiplets, as discussed in the next sections. Figure 4 shows the "clean Fourier transforms" for each year, with only the selected peaks. The bottom FT is a merger of all of them. The detected pulsation periods are listed in Table 13, Table 14, Table 15, Table 16 and Table 17. The *time of maximum* ($T_{\rm max}$) in the tables' last column is an instant when the pulsation reaches a maximum in amplitude. The times of maximum are computed in seconds from the BCT (Barycentric Coordinate Time) date T_o, given in the tables' caption.

The comparison of the clean FTs shows that most of the peaks with high amplitudes are persistent, appearing in all five FTs, but in all cases their amplitudes change, even taking into account their uncertainties (see Fig. 9). This shows that the amplitude of the pulsations modes are changing with time and sometimes their amplitude decrease below the detection limits. For this reason, to identify a large number of pulsation modes, it is necessary compare the clean FTs of several years.

6. The Period Spacing

The way the spacing in period is calculated and the identification of the pulsating mode is done follows a classical circular argument: first, we assume an initial period spacing for the ($\ell = 1$) modes, then we look for periods in the overlapped clean FT that fit it, then the period spacing is again calculated refining its initial value. The found periods are assumed be ($\ell = 1$, $m = 0$) modes and then we look for the lateral components ($\ell = 1$, $m = \pm 1$) of the triplets, consistent with the expected spacing caused by the rotational splitting. The peaks corresponding to identified modes are removed from the clean FTs and then we apply the same process to the remaining peaks to looking for ($\ell = 2$) pulsation modes. The remaining peaks that are not identified either as ($\ell = 1$) or as ($\ell = 2$) pulsation modes are discarded (in all cases, these peaks had low probability levels). Then, we look for peaks with lower probability levels (5 or 6) in the original FTs that fit the absent expected frequencies.

An initial value for the period spacings or, ΔP_ℓ, can be calculated from the Kolmogorov-Smirnov (K-S) test. Kawaler (1988) used the K-S test to study the spacing in the first eight periods detected by Winget et al. (1985) in the PG 1159-035 data. Later, Winget et al. (1991) also used the K-S test to estimate the mean spacing between the 122 detected periods in the 1989 WET data and found $\Delta P_1 = 21.50 \pm 0.03\,s$ (for $\ell = 1$ modes), and $\Delta P_2 = 12.67 \pm 0.03\,s$ (for $\ell = 2$ modes).

We applied the K-S test to our list of candidate pulsation periods. The result is shown in Fig. 5. The upper graph shows the

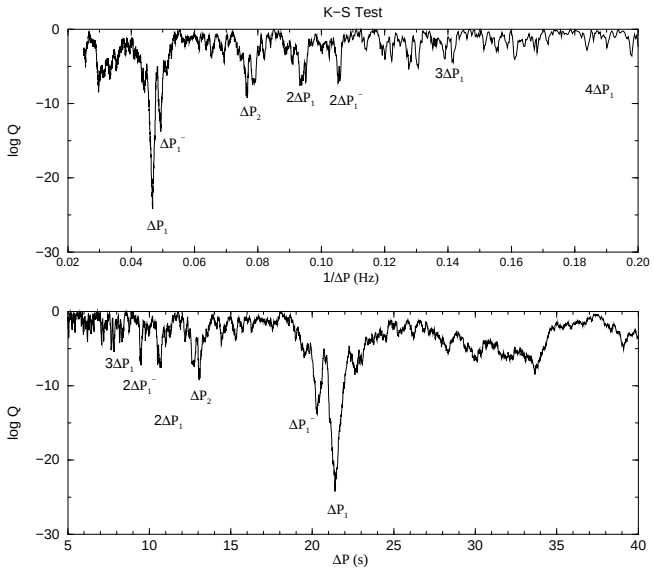

Fig. 5. The K-S applied to list of candidate pulsation periods.

Table 3. Spacing found by the K-S Test.

Spacing	(s)	(Hz)	log Q
ΔP_1	21.39	0.047	−21.4
ΔP_1^-	20.29	0.050	−20.3
ΔP_1^{--}	19.59	0.051	−3.2
ΔP_1^+	22.65	0.044	−8.1
ΔP_1^{++}	23.06	0.043	−6.8
ΔP_2	13.06	0.077	−9.1
ΔP_2^- ?	12.80	0.078	−7.4

confidence level (log Q) versus $1/\Delta P$, making the identification of harmonics in period spacings easier. The lower graph shows (log Q) versus ΔP (in seconds). The spacing ΔP_1 is 21.39 *s*, while ΔP_2 is 13.06 *s* (see Table 3). The ratio between the two values is $\Delta P_1/\Delta P_2 \simeq 1.638$, close to the expected $\sqrt{3}$. The difference around 5% is due, mainly, to the overlapping of the two sequences ($\ell = 1$ and $\ell = 2$).

An explanation for the structures of valleys (minima) revealed in the K-S test of Fig. 5 is illustrated in Fig. 6, where we can see all possible spacings between the peaks of two consecutive triplets (mode $\ell = 1$). The spacing between peaks of same m is ΔP, but there are greater spacings (ΔP^+ and ΔP^{++}) and shorter spacings (ΔP^- and ΔP^{--}). We must take into account that not all the the triplets frequencies are excited to detectable amplitudes. This can explain the lower and asymmetrical valleys around the valleys of ΔP_1 and ΔP_2 in Fig. 5 .

If the spacing between periods with same ℓ were exactly constant, the correct values for ΔP_1 and ΔP_2 would appear as sharp valleys in the K-S Test. The non-negligible width of the valleys indicate that the spacing is not exactly constant, having a certain deviation around ΔP_ℓ, as is theoretically expected and discussed in Sect. 13.

7. Mode Identification

In the FTs, the $\ell = 1$ and $\ell = 2$ sequences overlap. The identification of the periods with $\ell = 1$ is easier and more secure, because the spacing between them is large and they appear as triplets and not as higher multiplets. We used Eq.1 and the rotation period of the star, $P_{rot} = 1.38$ days, found by Winget et al.

Table 4. Identified $\ell = 1$ pulsation modes.

$k \pm 2$	m	Period (s)	Freq. (μHz)	Ampl. (mma)	Confid. Level	W91 (ℓ, m)	$k \pm 2$	m	Period (s)	Freq. (μHz)	Ampl. (mma)	Confid. Level	W91 (ℓ, m)
	+1	389.72	2565.94	0.2	5	29		+1	705.32	1417.80	0.8	1	1,+1
14	0	390.30	2562.13	1.0	1	2,-2	29	0	709.05	1410.34	0.3	5	1,0
	+1	390.84	2558.59	0.2	5	29		-1	711.58	1405.32	0.4	3	
	+1							+1	727.09	1375.36	0.7	1	1,+1
15	0	412.01	2427.13	0.6	1		30	0	729.51	1370.78	0.3	2	1,0:
	-1	413.14	2420.49	0.2	3			-1	731.45	1367.15	1.0	1	1,-1:
	+1	430.38	2323.53	0.3	5			+1	750.56	1332.34	1.6	1	
16	0	432.37	2312.83	0.5	3		31	0	752.94	1328.13	—	6	1,-1
	-1	434.15	2303.35	0.5	3			-1	755.31	1323.96	0.3	2	
	+1	450.83	2218.13	3.5	1	1,0:		+1					
17	0	452.06	2212.10	3.0	1		32	0	773.74	1292.42	0.3	3	1,0
	-1	453.24	2206.34	1.0	1	(1),?		-1	776.67	1287.55	0.4	3	1,-1
	+1							+1	790.26	1265.41	1.4		
18	0	472.08	2118.29	0.4	3		33	0	791.80	1262.95	—	6	
	-1	475,45	2103.27	0.3	3				793.34	1260.49	0.8	1	1,-1
	+1	493.79	2025.15	1.5	1	1,+1		+1	812.57	1230.66	0.4	2	2,?
19	0	494.85	2020.81	0.7	1	1,0	34	0	814.58	1227.61	0.4	3	1,+1
	-1	496.00	2016.13	0.2	3	1,-1		-1	817.40	1223.39	0.2	3	1,0
	+1	516.04	1937.83	7.2	1	1,+1		+1	835.34	1197.12	0.3	3	
20	0	517.16	1933.64	4.2	1	1,0	35	0	838.62	1192.44	0.6	1	1,0
	-1	518.29	1929.42	3.2	1	1,-1		-1	842.88	1186.41	1.0	1	1,-1
	+1	536.92	1862.47	0.5	1	1,+1		+1	857.37	1166.36	0.4	3	
21	0	538.14	1858.25	0.6	1	1,0	36	0	861.72	1160.47	0.5	3	
	-1	539.34	1854.12	1.0	1	1,-1		-1	865.08	1155.96	0.7	1	
	+1	557.13	1794.91	2.0	1	1,+1		+1	877.67	1139.38	0.4	5	
22	0	558.14	1791.67	2.4	1	1,0	37	0	883.67	1131.65	—	6	
	-1	559.71	1786.64	1.0	1	1,-1		-1	889.66	1124.02	0.3	1	
	+1	576.03	1736.02	0.1	5				898.82	1112.57	0.9	1	
23	0	579.12	1726.76	0.1	5	2,-1:	38	0	903.19	1107.19	0.7	1	
	-1	581.67	1718.18	0.1	5								
	+1	601.44	1662.66	0.3	5	1,+1		+1	923.19	1083.20	0.5	1	2(1),?
24	0	603.04	1658.25	0.2	5	1,0	39	0	925.31	1080.72	0.3	2	
	-1	604.72	1653.66	0.2	5	1,-1		-1	927.58	1078.07	0.5	3	
	+1	621.45	1609.07	0.2	5	1,+1		+1	943.01	1060.43	0.5	3	
25	0	622.00	1607.72	0.3	3	1,0	40	0	945.01	1058.19	0.3	3	
	-1	624/36	1601.64	0.3	5	1,-1		-1	947.41	1055.51	0.5	1	
	+1	641.54	1558.75	1.0	1	1,+1		+1	962.07	1039.43	0.3	3	
26	0	643.31	1554.46	0.5	1	1,0	41	0	966.98	1034.15	0.9	1	2(1),?
	-1	644.99	1550.41	0.8	1	1,-1		-1					
	+1	664.43	1505.34	0.3	3	1,+1		+1					
27	0	668.09	1496.80	0.3	3	1,-1	42	0	988.13	1012.01	0.2	3	2(1),-1:
	-1	672.21	1487.63	0.3	3			-1	994.12	1005.91	0.1	5	2(1),-2:
	+1	685.79	1458.17	0.3	2	1,+1							
28	0	687.74	1454.04	0.4	1	1,0							
	-1	689.75	1449.80	0.5	1	1,-1							

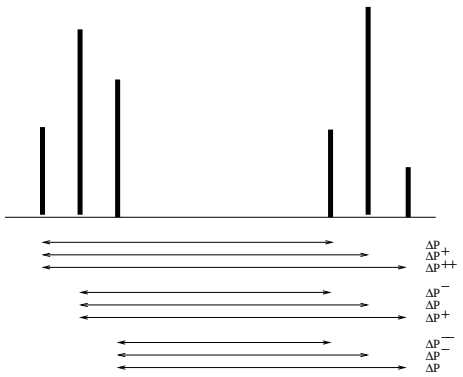

Fig. 6. Possible spacings between the components of two triplets.

(1991), to calculate the *approximate* position of the peaks of the triplets. The identification of the $\ell = 1$ pulsation modes is done by comparing the peaks in the FTs with the predicted positions. All peaks identified as $\ell = 1$ modes are listed in Table 4. For peaks present in more than one FT, the periods, frequencies and amplitudes in Table 4 are the average values.

We set the index k of each triplet assuming $k = 20$ for the triplet of 517 s, as calculated by Winget et al. (1991). Comparing the observed period spacing for $\ell = 1$ modes in the 1989 data set with models for pulsating PG1159 stars calculated by Kawaler and Bradley (1994) (hereinafter KB94), Winget et al. (1991) calculated that the triplet of 517 has index $k = 20 \pm 2$. The plot of period versus k is shown in Fig. 7. Fitting a straight line to the points, we can refine ΔP_1 and calculate ϵ [Eq. 1]:

$$\Delta P_1 = 21.43 \pm 0.03\ s \quad (3)$$

$$\epsilon = 88.05 \pm 21.43\ s \quad (4)$$

where, ϵ is the period for $k = 0$ (radial mode). Our result for ΔP_1 differs in $\sim 2\sigma$ from the value calculated by Winget et al. (1991).

Using the value for ϵ above and the initial estimate for ΔP_2 we started the investigation of the $\ell = 2$ sequence of pulsation modes. The indexes k for each $\ell = 2$ mode are calculated from Eq. 1 with an uncertainty of ± 2. The identified $\ell = 2$ modes are in Table 12 and the sequence of P as a function of k is shown in Fig. 7. The new computed value for ΔP_2 is:

$$\Delta P_2 = 12.38 \pm 0.01\ s \quad (5)$$

differing in $\sim 9\sigma$ from the value found by Winget et al. (1991), but the uncertainty in ΔP_2 can be underestimated, as explained later in this section. It is important to note that if the true index

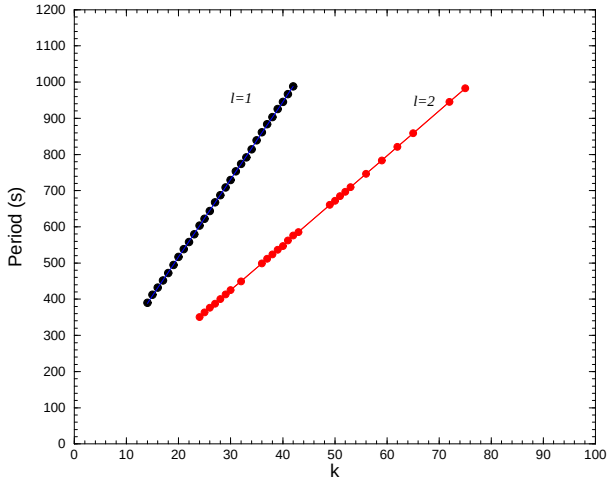

Fig. 7. Observed periods sequences for the modes $\ell = 1$ and $\ell = 2$.

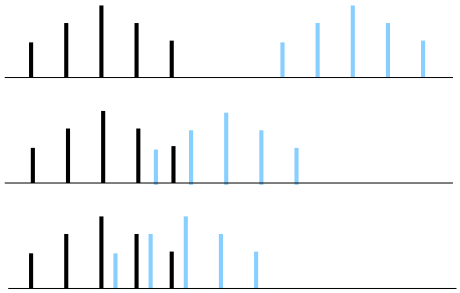

Fig. 8. Overlapping of two multiplets ($\ell = 2$). For periods less than 600 s, the overlappings do not occur. Between 600 – 750 s, there is the overlapping of only a peak and up to 750 s, the overlapping of two peaks.

for the 517 s triplet is $k \neq 20$, ϵ and the indexes k for the $\ell = 2$ sequence will need to be recalculated, but not ΔP_1 and ΔP_2. The ratio between the two period spacing is now closer to $\sqrt{3}$, the expected theoretical value,

$$\frac{\Delta P_1}{\Delta P_2} = \frac{21.43}{12.38} \simeq 1.731 \qquad (6)$$

differing by less than 0.06%. After the mode identification from the combined data, we used the modes with $m = 0$ to calculate ΔP_1 and ΔP_2 from each annual dataset. The results are shown in Table 12. (Note that some lines with no data were omitted only to short the table.)

The amplitudes of most $\ell = 2$ modes are very low and the absence of the multiplet components hinders the identification of the azimuthal index, m, of the other components. An additional complication is the overlapping of multiplets (see Fig. 8) which is more serious when k (and the period) increases. The multiplets with periods less than $\sim 600\,s$ appear isolated in the FTs of PG 1159-035. But, between ~ 600 and $\sim 750\,s$, the overlap of the more external components ($m = \pm 2$) occurs, and a component of one multiplet "invades" the space of the neighbor multiplet, and vice-versa. From periods of $\sim 750\,s$, there are overlaps of two components ($m = \pm 2$ and $m = \pm 1$). In the overlap regions, the mode identification is specially difficult and sometimes impossible, which explains the lack of continuity of period sequence in the curve for the $\ell = 2$ shown in Fig. 7. The overlap can also lead to the misidentification of the pulsation modes.

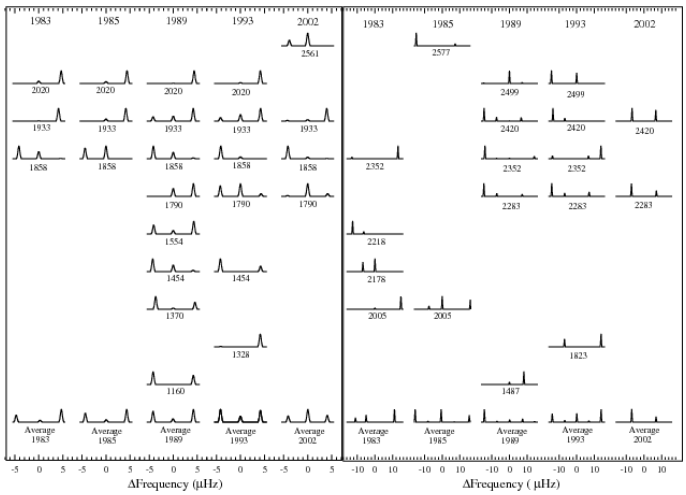

Fig. 9. Representation of $\ell = 1$ (left panel) and $\ell = 2$ (right panel) detected multiplets for the indicated years in the top of each panel. All the multiplets have at least two components. The number bellow each multiplet is its frequency in μHz. At the bottom of each panel are the average multiplets for each year. The heights of each multiplet peaks are normalized by the power of its highest peak.

For example, an "invader" $m = -1$ or $m = -2$ peak can have a period near to the expected period for the local $m = 0$ mode, being identified as the $m = 0$ mode of the local multiplet. This can explain why we obtained a better fitting for the $\ell = 2$ sequence than for the $\ell = 1$ sequence. In this case, the uncertainty in ΔP_2 is underestimated.

The columns "W91" in Table 4 and Table 12 show the mode identification, ℓ, m, as reported in Winget et al. (1991). Colons (:) after m indicate that other identification are possible. Modes in parenthesis, indicate a possible alternative identification. The symbol ? indicates when the index m is unknown. Most of the identifications obtained by us are the same as those by Winget et al. (1991).

8. The Splitting in Frequency

The observed splittings in frequency are caused by a combination of effects of the stellar rotation and the star's magnetic field. The magnetic splitting depends on the strength B and the geometry of the magnetic field of the star (Jones et al. 1989). For a symmetric magnetic field aligned to the pulsation symmetry axis, in first order,

$$\delta\nu_{\rm mag} \propto m^2 \gamma_k \; B^2 \qquad (7)$$

where γ_k is a proportionality constant which depends on the internal structure of the star, on the index k (and so, on the period), and on the shape of the magnetic field. If the rotation is slow ($P_{\rm rot} \gg P_{\rm puls}$) and if the rotation axis and the pulsation symmetry axis are approximately aligned, the rotational splitting is given by (Hansen et al. 1977):

$$\delta\nu_{\rm rot} = m\,(1 - C - C_1)\,\Omega_{\rm rot} + O(\Omega^2_{\rm rot}) + ... \qquad (8)$$

where $C = C(k, \ell)$ is the uniform rotation coefficient while $C_1 = C_1(k, \ell, |m|)$ contains the nonuniform rotation effects and

depends on the adiabatic pulsation properties, the equilibrium structure of the star, and the rotation law. In the asymptotic limit of high radial overtones, i. e., large values of k (Brickhill 1975), $C \approx 1/\ell(\ell+1)$; and, if we assume uniform rotation as a first approximation, $C_1 = 0$. If the second order terms in Eq.8 are neglected related to $\delta\nu_{\rm mag}$, then $\delta\nu_{\rm rot} \approx m\,\Omega_{\rm rot}$. While the rotation splits a g-mode in $(2\ell+1)$ components, an aligned magnetic field splits it only in $(\ell+1)$ components.

Figure 9 shows the triplets (left panel) and multiplets (right panel) with at least two detected components found in the FT of each annual data set. Assuming that the above mentioned conditions are true for PG 1159-035, the presence of multiplets with $(2\ell+1)$ peaks in its FT indicate that the rotational splitting is the dominant. To estimate $\delta\nu_{\rm rot}$ and $\delta\nu_{\rm mag}$ we calculated the $\delta\nu$ spacing in frequency between consecutive peaks of the Fig. 9 multiplets, and fitted to

$$\delta\nu \approx m\,\Omega_{\rm rot} + m^2\bar{\gamma}\,B^2 \qquad (9)$$

where $\bar{\gamma}$ is the average of γ_k. The spacings in frequency for the combined data $\ell = 1$ modes are $\delta\nu_{\rm rot,1} = 4.134 \pm 0.002$ μHz and $\delta\nu_{\rm mag,1} = 0.007 \pm 0.002$ μHz. The contribution of the magnetic splitting is less than 1%. For the $\ell = 2$ modes we found $\delta\nu_{\rm rot,2} = 6.90 \pm 0.01$ μHz. Unfortunately, the absence of peaks in the multiplets does not made it possible to estimate $\delta\nu_{\rm mag,2}$. Winget et al. (1991) analyzing only the PG 1159-035 1989 data set, found: $< \delta\nu_{\rm rot,1} >= 4.22 \pm 0.04$ μHz and $< \delta\nu_{\rm rot,2} >= 6.92 \pm 0.07$ μHz. Table 5 shows the rotational spacing in frequency for each data set.

9. The Rotational Period

For uniform rotation and asymptotic overtone limit in k, the rotation period in the region of period formation, $P_{\rm rot}$, can be calculated from the frequency spacing (Kawaler et al. 1999) as

$$P_{\rm rot} = \frac{1 - [\ell(\ell+1)]}{\delta\nu_{{\rm rot},\ell}} \qquad (10)$$

Calculating the $P_{\rm rot}$ mean value for $\ell = 1$ and $\ell = 2$, Winget et al. (1991) obtained $P_{\rm rot} = 1.388 \pm 0.013$ days. From our combined data, we obtained $P_{\rm rot} = 1.3930 \pm 0.0008$ days for $\ell = 1$ and $P_{\rm rot} = 1.3973 \pm 0.0022$ days. The two periods' average is $P_{\rm rot} = 1.3935 \pm 0.0008$ days, consistent with the previous value, but with a significative larger accuracy. The rotational periods calculated for each data set are shown in Table 5.

10. Inclination of the Rotational Axis

Theoretically, if the pulsational symmetry axis and the rotational axis are approximately aligned and if the amplitudes of all the pulsation modes of a multiplet are the same, the multiplets appear in the FT with a symmetrical design and the relative amplitudes of the components depend on the inclination angle, i, of the rotational axis (Pesnell 1985).

As noted by Winget et al. (1991), the PG 1159-035 multiplets do not have a symmetrical design and, as shown in Fig. 9, the relative powers (and amplitude) of the multiplets components change in time, but the average multiplets, shown in the bottom of the panels in Fig. 9, are approximately symmetrical relative to the central peak. From the average multiplets for the 1989 data set, Winget et al. (1991) estimated an inclination angle, $i \simeq 60^o$. In Fig. 10 the mean multiplets calculated from all the multiplets shown at Fig. 9 are shown. The relative powers of the peaks of the $\ell = 1$ *and* $\ell = 2$ average multiplets suggest a bit larger inclination angle, $i \simeq 70^o \pm 6^o$, but consistent with the previous result.

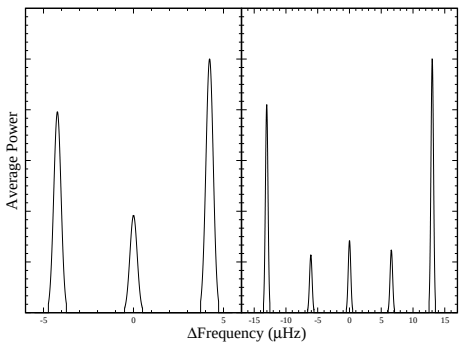

Fig. 10. Average multiplet for $\ell = 1$ (left panel) and for $\ell = 2$ (right panel) pulsation modes of PG 1159-035.

11. The Magnetic Field

If we assume any asymmetries in the splittings are due to magnetic filed effects, we can estimate an upper limit to the magnetic field. From the asymmetric in frequency splitting within a multiplet, $\delta\nu_{\rm mag}$, we are able to estimate an upper limit to the strength of the magnetic field, B, since $\delta\nu_{\rm mag} \approx m^2\,\gamma_k\,B^2$. We calculated the proportionality constant by scaling the results of Jones et al. (1989) for $\ell = 1$ modes (see their Fig.1), and obtained an upper limit $B < 2000$G, with a average value $B \sim 1200$G. Our upper limit for B is three times less than the one found by Winget et. al. (1989), of 6000 G. Vauclair et al. (2002) found the limit $B < 500$ for another PG 1159 star, the hot RXJ 2117+3212. As observed by Vauclair too, the estimates of the upper limit for B are taken from the calculations for a pure carbon white dwarf star by Jones et al. (1989), and it can only be an approximated value when scaled to PG 1159-035.

12. Mass Determination

The mass is the stellar parameter with largest impact on the internal structure and evolution of the stars. However, with exception of a small fraction of stars belonging to binary systems, the mass cannot be obtained by direct observation. The mass of (pre-)white dwarf stars can be spectroscopically estimated, from the comparison of the observed spectrum with theoretical spectra predicted by stellar atmospheric models (spectroscopic mass). For the pulsating stars, the mass can also be asteroseismologically derived by way of the comparison of the observed spacing in the star's pulsation periods and the ones predicted by pulsation models (seismic mass).

12.1. KB94 Parameterization

From ΔP_1 and ΔP_2 derived in 6, the proportionality constant P_o in Eq.2 may be calculated:

$$P_o = \sqrt{\ell(\ell+1)}\,\Delta P_\ell \qquad (11)$$

Table 5. Results for each annual data set.

Data set	1983	1985	1989	1993	2002	Combined	W91
ΔP_1 (s)	21.31 ± 0.06	21.44 ± 0.04	21.36 ± 0.04	21.49 ± 0.03	21.24 ± 0.06	21.43 ± 0.03	21.50 ± 0.03
ΔP_2 (s)	12.41 ± 0.05	12.36 ± 0.04	12.38 ± 0.02	12.38 ± 0.03	12.38 ± 0.04	12.38 ± 0.01	12.67 ± 0.03
$\delta\nu_1$ (μHz)	4.133 ± 0.003	4.133 ± 0.005	4.167 ± 0.006	4.177 ± 0.007	4.152 ± 0.014	4.153 ± 0.002	4.22 ± 0.04
$\delta\nu_2$ (μHz)	6.80 ± 0.02	—	7.01 ± 0.03	6.96 ± 0.02	6.81 ± 0.08	6.903 ± 0.011	6.92 ± 0.07
$P_{\mathrm{rot},\ell=1}$ (d)	1.400 ± 0.001	1.400 ± 0.002	1.389 ± 0.002	1.386 ± 0.002	1.394 ± 0.005	1.3934 ± 0.0008	1.371 ± 0.13
$P_{\mathrm{rot},\ell=2}$ (d)	1.418 ± 0.004	—	1.376 ± 0.005	1.385 ± 0.003	1.417 ± 0.016	1.3973 ± 0.0022	1.388 ± 0.013
P_{rot} (d)	1.401 ± 0.001	1.300 ± 0.002	1.387 ± 0.002	1.386 ± 0.002	1.396 ± 0.005	1.3939 ± 0.0008	1.38 ± 0.01
$E_{\ell=1}$ ($\times 10^{-8}\,\mu$Hz^2)	3.10 ± 0.07	2.06 ± 0.08	2.37 ± 0.02	2.38 ± 0.03	2.17 ± 0.03	—	—
$E_{\ell=2}$ ($\times 10^{-8}\,\mu$Hz^2)	1.630 ± 0.002	1.015 ± 0.002	0.867 ± 0.007	0.873 ± 0.006	1.011 ± 0.010	—	—
E_{tot} ($\times 10^{-8}\,\mu$Hz^2)	4.730	3.077	3.240	3.257	3.176	—	—
$E_{\ell=1}/E_{\mathrm{tot}}$	0.66	0.67	0.73	0.73	0.68	—	—

For $\ell = 1$, $P_o = 30.31 \pm 0.04$ s and for $\ell = 2$, $P_o = 30.32 \pm 0.03$ s. The weighted average is:

$$P_o = 30.32 \pm 0.03 \quad (s) \tag{12}$$

The previous result (KB94) is $P_o = 30.5 \pm 3.0$. The constant P_o depends on the internal structure of the star (see, e.g., Shibahashi 1988):

$$P_o = 2\pi^2 \left(\int \frac{N(r)}{r} dr \right)^{-1} \tag{13}$$

where, $N(r)$ is the *Brunt-Väisälä frequency* and the integration is done over all the region of propagation of the g-modes inside the star. From the parameterization of a grid of models, KB94 found an expression for P_o as a function of three stellar parameters, the stellar mass (in $M_\odot$), M; the luminosity (in $L_\odot$), L; and the fractional mass of the helium superficial layer, q_{Y}:

$$P_o = z \left(\frac{M}{M_\odot} \right)^a \left(\frac{L}{L_\odot} \right)^b q_{\mathrm{Y}}^c \tag{14}$$

where, z, a, b and c are constants. Knowing P_o, L, q_{Y} and the four constants above, the stellar mass can be determined:

$$\frac{M}{M_\odot} = \left(\frac{P_o}{z} \right)^{1/a} \left(\frac{L}{L_\odot} \right)^{-b/a} q_{\mathrm{Y}}^{-c/a} \tag{15}$$

The general equation to estimate the uncertainty, σ_{M}, in the mass determination is

$$\sigma_{\mathrm{M}} = \frac{M}{|a|} \left[\left(\frac{\sigma_{\mathrm{P_o}}}{P_o} \right)^2 + \left(b \frac{\sigma_{\mathrm{L}}}{L} \right)^2 + \left(c \frac{\sigma_{\mathrm{q_Y}}}{q_{\mathrm{Y}}} \right)^2 + \left(\frac{\sigma_{\mathrm{z}}}{z} \right)^2 + \right. \tag{16}$$
$$\left. + \; (\ln (M/M_\odot)\; \sigma_{\mathrm{a}})^2 + (\ln (L/L_\odot)\; \sigma_{\mathrm{b}})^2 + (\ln (q_{\mathrm{Y}})\; \sigma_{\mathrm{c}})^2 \right]^{1/2}$$

The equation above take into account the contribution of all parameters of Eq.14, but the last term is the dominant one and all other terms can be neglected. Then,

$$\sigma_{\mathrm{M}} \simeq M \left| \frac{ln\,(M/M_\odot)}{a} \right| \sigma_{\mathrm{a}} \tag{17}$$

For PG1159 stars, KB94 calculated $z = 18.196$ sec, $a = -1.3$, $b = -0.035$ and $c = -0.00012$ with $L = (195 \pm 3)\,L_\odot$, $q_{\mathrm{Y}} = 0.039$ and obtained $M/M_\odot = 0.59 \pm 0.01$ for PG 1159-035. The uncertainty for a was not published, but if we assume that the σ_{a} is of the same order of the last significant digit of a, $\sigma_{\mathrm{a}} \simeq 0.1$, and use our result for P_o, we obtain $M/M_\odot = 0.59 \pm 0.02$, while Winget et al. (1991) found $M/M_\odot = 0.586 \pm 0.003$. The difference in the uncertainties for $M/M_\odot$ is probably because Winget assumed a smaller value for σ_{a}, in spite of our higher accuracy in the measured $\sigma_{\mathrm{P_o}}$. The dominant uncertainty in the mass determination is the theoretical models, not the observations.

12.2. New Asteroseismological Models

Córsico et al. (2006) performed an extensive g-mode stability analysis on PG1159 evolutionary models, considering the complete evolution of their progenitors, obtaining $M/M_\odot \simeq 0.536$ for PG 1159-035. They point out that for this mass and at the effective temperature of PG 1159-035, their analysis predicts that the model is pulsationally unstable, but with a period spacing of $\Delta P_1 \simeq 23$s, which is in conflict with the observed $\Delta P_1 = 21.43$s. To have a ΔP_1 compatible with the observed one, the mass of PG 1159-035 should be $M/M_\odot \simeq 0.558$, 1.6σ less than our result. They suggest that improvements in the evolutionary codes for the thermally pulsing AGB phase and/or for the helium burning stage and early AGB could help to alleviate the discrepancies between the spectroscopic mass and the mass calculated from the period spacing.

Preliminary results of a detailed asteroseismological study on PG 1159-035 on the basis of an enlarged set of full PG1159 evolutionary models (Córsico et al. 2007 in preparation) indicate that the PG 1159-035 stellar mass is either $\approx 0.585 M_\odot$ (if the star is on the rapid contraction phase before reaching its maximum effective temperature) or $\approx 0.577 M_\odot$ (if the star has just settled onto its cooling track). These inferences are derived from a comparison between the observed period spacing and the asymptotic period spacing. This range in mass is in agreement with the value of $M_\star \approx 0.59 M_\odot$ derived by Winget al. (1991) and KB94 — and also in agreement with the value derived in the present paper from the KB94 parameterization — on the basis of an asymptotic analysis.

We must emphasize, however, that the derivation of the stellar mass using the asymptotic period spacing is not entirely reliable in the case of PG1159 stars. This is because the asymptotic predictions are strictly valid for chemically homogeneous stellar models, while PG1159 stars are expected to be chemically stratified, characterized by pronounced chemical gradients built up during the progenitor star life. A more realistic approach to infer the stellar mass of PG1159 stars is to compare the average of the computed period spacings ($\overline{\Delta P_\ell}$) with the observed period spacing. To this end, we computed adiabatic nonradial g-modes and evaluated $\overline{\Delta P_\ell}$ by averaging the computed forward period spacings ($\Delta P_k = P_{k+1} - P_k$, k being the radial order) in the appropriate range of the observed periods in PG 1159−035. At the observed effective temperature we find two solutions for the PG 1159-035 stellar mass: $\approx 0.586 - 0.587 M_\odot$ and $\approx 0.56 - 0.57 M_\odot$, depending on its location on the HR diagram[1]. We can safely discard

[1] Note that these values are somewhat different from the mass derived in Córsico et al. (2006) because in that paper the authors used a different range of periods to compute $\overline{\Delta P_\ell}$, and older values for the period spacing.

the solution before the knee $M_* \approx 0.586 - 0.587 M_\odot$ because the predicted surface gravity is much lower ($\log g \approx 6$) than the spectroscopically inferred value $\log g = 7.0 \pm 0.5$. Thus, our best estimate for the mass of PG 1159-035 is $\approx 0.56 - 0.57 M_\odot$. We postpone to a later publication (Córsico et al. 2007) a detailed asteroseismological study based on a fitting to the individual observed periods in PG 1159-035.

12.3. Spectroscopic Mass

The stellar mass can also be spectroscopically estimated from the comparison of optical and/or UV spectra of the star with results of atmospheres models. Using line blanketed NLTE model atmospheres, Dreizler and Heber (1998) found $M/M_\odot = 0.54$ for PG 1159-035. The same result was obtained by Miller Bertolami and Althaus (2006) from full evolutionary models for post-AGB PG1159 stars.

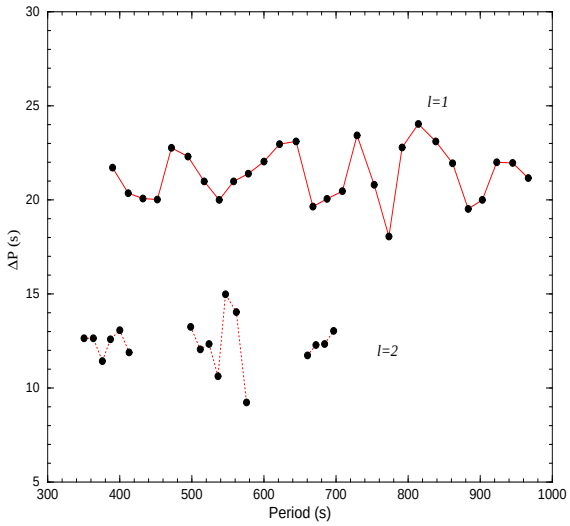

Fig. 11. ΔP diagram for PG 1159-035.

13. Trapped Modes

The asymptotic approximation of the Eq.1 calculates with excellent precision the pulsation periods for completely homogeneous models for PG1159 stars. However, the inner composition of pre-white dwarfs changes between the core of C/O and the superficial layer, rich in helium. The regions where the gradient of the inner composition drastically changes are called *transition zones*. These zones can work as a reflection wall for certain pulsation modes, isolating them into specific regions of the star, as in a resonance box. This way, the modes can be "trapped" inside the core of C/O, as well as, between the stellar surface and the transition zone.

The trapping of pulsation modes changes the spacing between consecutive periods relative to the uniform spacing, ΔP_ℓ. The analysis of the deviations from the uniform period spacing allows us to study the trapping of pulsation modes inside the star and obtain some relevant information about its internal structure. The main tool in this analysis is the ΔP diagram, a graph of the local spacing, $\Delta P = P_{k+1} - P_k$, versus the period P_k of the $m = 0$ modes. Figure 11 shows the ΔP diagram for PG 1159-035 using the $m = 0$ modes listed in Table 6. The $\ell = 1$ sequence between $k = 14$ and $k = 41$ is complete, while the $\ell = 2$ sequence is incomplete. Fortunately, the most significant information can be obtained from the $\ell = 1$ sequence alone. The ($\ell = 1$) trapped modes appears as points of minimum in the ΔP diagram (KB94) and are listed in Table 7. We note that, with exception of the mode of 452s which has amplitude $\simeq 3$ mma, all other trapped modes have relatively low amplitudes ($\lesssim 0.6$ mma).

Table 6. Points in the ΔP diagram.

$\ell = 1$			$\ell = 2$		
$k \pm 2$	P (s)	ΔP (s)	$k \pm 2$	P (s)	ΔP (s)
14	390.30	21.71	24	350.75	12.64
15	412.01 *[a]	20.36	25	363.39	12.64
16	432.37 *	20.07	26	376.03	11.44
17	452.44	20.02	27	387.47	12.59
18	472.08 *	22.77	28	400.06	13.08
19	494.85	22.31	29	413.14 *	11.90
20	517.16	20.98	36	498.73	13.25
21	538.14	20.00	37	511.98	12.05
22	558.14	20.98	38	524.03	12.34
23	578.61	21.39	39	536.37	10.63
24	600.00 *	22.03	40	547.00	14.99
25	622.03 *	22.96	41	561.99	14.03
26	644.99	23.10	42	576.02	9.24
27	668.09	19.65	49	660.46	11.74
28	687.74	20.06	50	672.20	12.28
29	709.05 *	20.46	51	684.48	12.35
30	729.51	23.43	52	696.83	13.04
31	752.94	20.80			
32	773.74	18.06			
33	791.80	22.78			
34	814.58	24.04			
35	838.62	23.10			
36	861.72 *	21.95			
37	883.67	19.52			
38	903.19 *	20.00			
39	923.19 *	22.00			
40	945.01	21.97			
41	966.98	21.15			

[a] The asterisk * indicates unsure mode identification.

Table 7. Trapped modes ($\ell = 1$).

i	Period (s)
1	452.431 ± 0.002
2	538.154 ± 0.003
3	668.071 ± 0.024
4	773.744 ± 0.064
5	883.637 ± 0.122

14. Transition Zone

As the trapping of the pulsation modes depends on the resonance between the eigenfunctions for the pulsations and the depth of the transition zone, the periods for which the modes are trapped are sensitive to the geometric depth, r_c, of the transition zone. The periods of the trapped modes can be calculated by the analytical approximation, originally proposed by Carl J. Hansen:

$$P_i^2 \simeq 4\pi^2 \lambda_i^2 \left[\left(1 - \frac{r_c}{R_\star} \right) \ell(\ell+1) \frac{GM}{{R_\star}^3} \right]^{-1} , \qquad (18)$$

where, λ_i are constants related with the zeros of the Bessel functions; r_c is the position of the transition zone; and P_i is the period of the trapped mode which has i nodes between the stellar surface ($r = R_\star$) and the transition zone ($r = r_c$).

The constants λ_i are called *trapping coefficients* and are empirically calculated from models for white dwarfs and pre-white dwarfs by several groups. Table 8 shows the coefficients λ_i for $i = 0 - 9$ for the models of PG 1159 calculated by Bradley and Winget (1991).

Table 8. Trapping coefficients for PG1159 models.

i	λ_i[a]
0	3.33 ± 0.10
1	4.92 ± 0.16
2	6.15 ± 0.18
3	7.45 ± 0.16
4	8.76 ± 0.06
5	10.17 ± 0.18
6	11.46 ± 0.18
7	12.77 ± 0.19
8	13.82 ± 0.35
9	15.26 ± 0.26

[a] Source: Kawaler and Bradley (1990).

Table 9. Ratios between the observed trapped periods.

	538.14s	668.09s	773.74s	883.67s
452.44s	1.189	1.477	1.710	1.953
538.14s	—	1.241	1.438	1.643
668.09s	—	—	1.158	1.323
773.74s	—	—	—	1.142

Table 10. Values for $r_c/R_\star$ for each trapped mode of PG 1159-035 ($R/R_\odot = 0.025 \pm 0.005$).

i	P_i (s)	λ_i	$r_c/R_\star$
1	452.431002	4.92	0.84 ± 0.05
2	538.153994	6.15	0.83 ± 0.06
3	668.070986	7.45	0.83 ± 0.05
4	773.744021	8.76	0.83 ± 0.02
5	883.635988	10.17	0.82 ± 0.06

From the Eq.18, the ratio between two periods, $P_i > P_j$, is given by:

$$\frac{P_i}{P_j} = \frac{\lambda_i}{\lambda_j} \quad \text{with } i > j \, . \tag{19}$$

The first step is to identify the indexes i and j. Table 9 shows all ratios for $P_k/P_{k'}$, with $k > k'$, for the trapped modes of PG 1159-035, while Table 11 shows the ratios between λ_i/λ_j with $i > j$. From the comparison of the two tables, we found that the sequence of indexes that best fit is $i = 1, 2, 3, 4, 5$. We point out that the identification of the trapped indexes, i, (fortunately) does not require exact identifications of the radial indexes, k.

For $\ell = 1$, the expression in Eq.18 becomes:

$$P_i^2 = 2\pi^2 \lambda_i^2 \left[\left(1 - \frac{r_c}{R_\star} \right) \frac{GM}{{R_\star}^3} \right]^{-1} \quad , \tag{20}$$

and we obtain:

$$r_c/R_\star = \left(1 - \frac{2\pi^2 \lambda_i^2}{GMP_i^2} {R_\star}^3 \right) \tag{21}$$

For positive values for $r_c/R_\star$, the radius of the star, $R_\star$, must be $R_\star < 0.045\, R_\odot$. Using $M/M_\odot = 0.59$ and assuming $R/R_\odot = 0.025 \pm 0.005$ (KB94), we can calculate r_c for each trapped mode of PG 1159-035 , as shown in Table 10. All results are concentrated around $0.83\, R_\star$, with small dispersion:

$$r_c/R_\star = 0.83 \pm 0.05 \quad . \tag{22}$$

Theoretical models calculated by Paul Bradley for PG 1159 stars derived from standard post-asymptotic giant branch (AGB) stellar models (see KB94 for a detailed description), and fitted to (PG 1159-035) data with radio $R_\star = 0.026\, R_\odot$, calculate that the position of the transition zone between the core of C/O and the He layer is between 0.60 and 0.65 $R_\star$, which differ from our value by a factor of $\sim 4\sigma$. This discrepancy suggest that the assumed parameters in the models are not the best ones for PG 1159-035, if the trapping occurs at the He to C/O transition.

15. Linear Combinations of Frequencies

There is no evidence of linear frequency combination involving the almost 200 pulsation frequencies in PG 1159-035. The presence of peaks in the FT resulting of linear combinations of frequencies indicates a nonlinear behavior. Linear combinations of frequencies have been observed in DAVs and in DBVs. It is the case of the DAV star GD 154 (Pfeiffer et al. 1996) and the DBVs stars GD 358 (Vuille et al. 2000 and Kepler et al. 2003).

The physical causes of the nonlinear behavior are not well understood. But, perhaps, PG 1159-059 is giving us a hint: a difference between PG1159 stars, and all other pulsating white dwarf stars is that DAVs and DBVs have convective layers, while PG1159 stars do not have significant ones. This fact is an indirect support to the hypothesis that the origin of the nonlinear behaviors be the convection, as was proposed by Brickhill (1990, 1992), Goldreich and Wu (1999a, 1999b), Weidner and Koester (2003), and Montgomery (2005).

16. Power Conservation

The kinetic energy of oscillation, $E_{\rm kin}$, is defined by

$$E_{\rm kin} = \frac{\sigma^2}{2} \int_0^{M_\star} |\delta \boldsymbol{r}|^2 dM_r \tag{23}$$

$$= \frac{\sigma^2}{2} I_{k\ell} \tag{24}$$

where $\sigma = 2\pi\nu$ is the angular eigenfrequency, $\delta \boldsymbol{r}$ is the Lagrangian displacement vector, $I_{k\ell} \equiv \int_0^{M_\star} |\delta \boldsymbol{r}|^2 dM_r$, and the relative radial displacement is normalized to $\delta r/r = 1$ at the stellar surface. Since modes with the same surface amplitude can have very different $I_{k\ell}$ values, we can only calculate total kinetic energies if we have a numerical model of the star with which to calculate these quantities.

If we only want to compare the surface kinetic energy densities of different modes, however, we can do a bit better than this. Ignoring geometric factors throughout this derivation, we have $E_{\rm kin} \propto \sigma^2 \xi_h^2$, where ξ_h is the horizontal displacement at the surface. From Robinson, Kepler, & Nather (1982), we find that

$$\frac{\delta F}{F} \propto \frac{1}{\sigma^2} \frac{\delta r}{r} \tag{25}$$

Assuming the Cowling approximation and that the oscillations are adiabatic at the surface, we have (e.g., Unno et al. 1989)

$$\frac{\xi_h}{\delta r} \propto \frac{1}{\sigma^2}, \tag{26}$$

which, combined with the previous result yields

$$\frac{\delta F}{F} \propto \frac{\xi_h}{r}. \tag{27}$$

Thus,

$$E_{\rm kin} \propto \sigma^2 \xi_h^2 \propto \sigma^2 \left(\frac{\delta F}{F} \right)^2 \tag{28}$$

Table 11. Ratios λ_i/λ_j, with $i > j$.

	λ_1	λ_2	λ_3	λ_4	λ_5	λ_6	λ_7	λ_8	λ_9
λ_0	1.477	1.847	2.237	2.630	3.054	3.441	3.835	4.150	4.583
λ_1	—	1.331 [a]	1.514	1.780	2.067	2.329	2.596	2.809	3.102
λ_2	—	—	1.211	1.424	1.654	1.863	2.076	2.247	2.481
λ_3	—	—	—	1.176	1.365	1.538	1.714	1.855	2.048
λ_4	—	—	—	—	1.161	1.308	1.458	1.578	1.742
λ_5	—	—	—	—	—	1.127	1.256	1.358	1.500
λ_6	—	—	—	—	—	—	1.114	1.206	1.332
λ_7	—	—	—	—	—	—	—	1.802	1.195
λ_8	—	—	—	—	—	—	—	—	1.104

[a] The rations in the boxes are those ones than best fit to rations between the observed trapped periods, shown in Table 9.

$$\propto \nu^2 A^2. \quad (29)$$

The total surface kinetic energy of the oscillations is the sum of the individual surface kinetic energies of all the pulsation modes:

$$E_{\rm kin} \propto \sum_i {\nu_i}^2 A_i^2 \quad (30)$$

where ν_i are the frequencies (in units of $\times 10^{-8}\mu$Hz) and A_i are the observed photometric mode amplitudes. The total kinetic oscillation energy for the observed $\ell = 1$ and $\ell = 2$ pulsation modes in PG 1159-035 is shown in Table 5, in terms of $\times 10^{-8}\mu$Hz^2. The arithmetic means of the kinetic oscillation energy for the $\ell = 1$ and $\ell = 2$ pulsation modes are $E_1 = 2.4 \pm 0.4$ and $E_2 = 1.1 \pm 0.4$. and $E_{\rm tot} = E_1 + E_2 = 3.5 \pm 0.6$. The deviations relative to the mean value year to year are less than 30% for E_1, less than 50% for E_2 and less than 35% for $E_{\rm tot}$. With exception of 1989 and 1993 (our best datasets) the deviations are larger than the uncertainties in E_1 and E_2, suggesting that the total surface kinetic energies are not conserved. For all data sets, E_1 corresponds to 65 – 75% of the detected modes total energy, $E_{\rm tot}$, not correcting for geometrical effects.

17. Conclusions and Comments

Winget et al. (1991), analyzing the WET 1989 data set of PG 1159-035, found 122 pulsation modes, with frequencies between 1000 and 3000 μHz in the star's FT, with a spacing in period of $\Delta P_1 = 21.50 \pm 0.03$ s and $\Delta P_2 = 12.67 \pm 0.03$ s. The seismological mass calculated from the spacing in period and using a theoretical model for a PG 1159 star was $M/M_\odot = 0.586 \pm 0.003$. The analysis of the fine structure of the multiplets shown a spacing in frequency $\delta\nu_{\rm rot,1} = 4.22 \pm 0.04\mu$Hz and $\delta\nu_{\rm rot,2} = 6.92 \pm 0.07\mu$Hz for $\ell = 1$ and $\ell = 2$ modes, respectively, which allowed the calculation of the star's rotation period, $P_{\rm rot} = 1.38 \pm 0.01$ days; of the rotation axis inclination, $i \sim 60^o$; and to estimate an upper limit for the magnetic strength, $B < 6000$ G.

In this work, we followed the same steps of Winget, but using a larger number of data sets and improved data reduction and data analysis techniques. The combination of the Fourier transforms of the data sets from different years (1983, 1985, 1989, 1993 and 2002) allows us to refine the determination or put new constraints over several stellar parameters of PG 1159-035. Our main results are:

1. We identified 76 new pulsation modes, increasing to 198 the total number of known pulsation modes for PG 1159-035. Only 14 of them (all with $\ell = 1$) are present in the FTs of all the years, but with different amplitudes. The comparison of the annual FTs shows that the amplitudes of the pulsation modes are changing in time, and can reach amplitudes below our detection limits. No evidence of $\ell > 2$ modes was found in the combined FTs of all the years.
2. The period spacings are $\Delta P_1 = 21.43 \pm 0.03\,s$ for $\ell = 1$ modes and $\Delta P_2 = 12.38 \pm 0.01\,s$ for $\ell = 2$ modes. The period constant, $P_o = \sqrt{\ell(\ell+1)}\,\Delta P_\ell$, is $P_o = 30.32 \pm 0.03$ sec.
3. We found a mass $M/M_\odot = 0.59 \pm 0.02$ from the KB94 parameterization. The apparent lower accuracy in the mass determination relative to the Winget determination, although we have substantially decreased the uncertainty in P_o, is because we took into account the dominant uncertainty in the theoretical models. As pointed out by Winget, the stated error in their determination of the PG 1159-035 mass reflects only the uncertainty in the measured period spacing, and not the systematic errors associated to the models. In this sense, even though our result is formally less accurate, it is more realistic.
4. Analyzing the spacing in frequency inside the multiplets we found that the splitting due to the stellar rotation is $\delta\nu_{\rm rot,1} = 4.154 \pm 0.002\mu$H for $\ell = 1$ modes and $\delta\nu_{\rm rot,2} = 6.90 \pm 0.01\mu$Hz for $\ell = 2$ modes.
5. We also estimated that the splitting in frequency due to the magnetic field for $\ell = 1$ modes is $\delta\nu_{\rm mag,1} = 0.007 \pm 0.002\mu$Hz, contributing with less than 1% of the total splitting. Unfortunately, it was not possible to calculate the magnetic spacing in frequency for the $\ell = 2$ modes, due to the absence of several components in the multiplets.
6. From the rotational frequency splitting we calculated the rotational period $P_{\rm rot} = 1.3920 \pm 0.0008$ days.
7. The magnetic splitting in frequency suggests a upper limit for the magnetic strength lower than the previous estimates: $B \lesssim 2000$ G.
8. The analysis of the fine structure of the combined data multiplets ($\ell = 1$ *and* $\ell = 2$) suggests that the inclination angle of the rotational axis is $i \sim 70^o \pm 6^o$.
9. The ΔP diagram of PG 1159-035 for $\ell = 1$ modes suggests that PG 1159-035 is already a stratified star. The ΔP diagram presents five minima that can be interpreted as the indication of trapped modes with periods of 452.43s, 538.12s, 668.1s, 773.7s and 883.6s.
10. For this sequence of trapped modes, we calculated the position of the transition zone that causes the trapping mode at $r_c/R_\star = 0.83 \pm 0.05$ for a star with $M/M_\odot = 0.59$ and $R_\star/R_\odot = 0.025$.

11. There is no evidence of linear combinations of frequencies in PG 1159-035. As models of PG 1159-035 do not have any significant convective layer, this provides indirect support to the hypothesis that nonlinearity arises in the convection zone.
12. Comparing the total power of the pulsation modes of the different years between 1983 and 2002, we observe that the differences relative to the mean value are less than 30% for the $\ell = 1$ modes and less than 50% for the $\ell = 2$ modes, indicating that the total surface kinetic energies are not conserved.

In continuation to the present work, we measured the temporal changing of the pulsation period ($\dot{P}$) of several pulsation modes in PG 1159-035. As PG 1159-035 is a very hot star, it is quickly evolving and its pulsation periods are changing in time. The period changes are large enough to be directly measured and for some we can derive the second order temporal variation ($\ddot{P}$). The results are presented in a separated paper (Costa et al. 2007).

We are currently performing a detailed asteroseismological study on PG 1159-035 based on an enlarged set of full PG1159 evolutionary models. Preliminary results, obtained from the comparison of the average period spacings of the models and of the observed periods, suggest that the mass of PG 1159-035 is $\approx 0.56 - 0.57\, M_{\odot}$ (see Sect.12.2). The next step is to fit the models to the individual observed periods in PG 1159-035. This study will be published in a separated paper (Córsico et al. 2007 in preparation).

Acknowledgements. This work was partially supported by CNPq-Brazil, NSF-USA and MCyT-Spain. In particular, M. H. Montgomery was supported by NSF grant AST-0507639.

References

Barstow, M. A., Holberg, J. B., Grauer, A. D. and Winget, D. E. 1986, ApJ, 306, L25

Bradley, P. A. and Winget, D. E. 1991, ApJS, 75, 463

Brassard, P., Fountaine, G., Wesemael, F. and Tassoul, M. 1999, ApJS, 81, 747

Breger, M., Handler, G. 1993, Balt. Ast., 2, 468

Brickhill, A. J. 1990, MNRAS, 246, 510

Brickhill, A. J. 1992, MNRAS, 259, 519

Bruvold, A., 1993, Balt. Ast., 2, 530

Córsico, A. H., Althaus, L. G. and Miller Bertolami, M. M. 2006, A&A, 458, 259

Córsico, A. H. et al. in preparation.

Costa, J. E. S. and Kepler, S. O., 1995, Balt. Ast., 4, 334

Costa, J. E. S. and Kepler, S. 0., 1999, Balt. Ast., 9, 451

Costa, J. E. S., Kepler, S. O. and Winget, D. E. 1999, ApJ, 522, 973

Costa, J. E. S., Kepler, S. O., Winget, D. E., O'Brien, M. S., Bond, H. E., Kawaler, S. D. and Dreizler, S. 2003, Balt. Ast. , 12, 23

Costa, J. E. S. and Kepler, S. O. 2007, in preparation.

Dreizler, S. and Heber, U. 1998, A&A, 334, 618

Goldreich, P. and Wu, Y. 1999a, AJ, 511, 904

Goldreich, P. and Wu, Y. 1999B, AJ, 523, 805

Green, R. F., Schmidt, M. and Liebert, J. 1986, ApJ, 61, 305

Jahn, D., Rauch, T., Reiff, E., Werner, K., Kruk, J. W. and Herwig, F. 2007, A&A, 462, 281

Jones, P.W., Pesnell, W.D., Hansen, C.J. and Kawaler, S.D. 1989, ApJ, 336, 403

Kawaler, S. D. 1986, PhD. Thesis. Univ. Texas at Austin

Kawaler, S. D. 1988, ApJ, 334, 220

Kawaler, S. D. and Weiss, P. 1990, in *Lecture Notes in Physics*, 367, 431

Kawaler, S. D. and Bradley, P. A. 1994, ApJ, 427, 415 (KB94)

Kawaler, S. D., Sekii, T., and Gough, D. 1999, ApJ, 516, 349

Kepler, S. 0. 1993, Balt. Ast., 2, 515

Kepler, S. O., Giovannini, O., Wood, M. A., Nather, R. E., Winget, D. E., Kanaan, A., Kleinman, S. J., Bradley, P. A., Provencal, J. L., Clemens, J. C., Claver, C. F., Watson, T. K., Yanagida, K., Krisciunas, K., Marar, T. M. K., Seetha, S., Ashoka, B. N., Leibowitz, E., Mendelson, H., Mazeh, T., Moskalik, P., Krzesinski, J., Pajdosz, G., Zola, S., Solheim, J.-E., Emanuelsen, P.-I., Dolez, N., Vauclair, G., Chevreton, M., Fremy, J.-R., Barstow, M. A., Sansom, A. E., Tweedy, R. W., Wickramasinghe, D. T., Ferrario, L., Sullivan, D. J., van der Peet, A. J., Buckley, D. A. H. and Chen, A.-L. 1995, ApJ, 447, 874

Kepler, S. O., Nather, R. E., Winget, D. E., Nitta, A., Kleinman, S. J., Metcalfe, T., Sekiguchi, K., Xiaojun, Jiang, Sullivan, D., Sullivan, T., Janulis, R., Meistas, E., Kalytis, R., Krzesinski, J., Ogoza, W., Zola, S., O'Donoghue, D., Romero-Colmenero, E., Martinez, P., Dreizler, S., Deetjen, J., Nagel, T., Schuh, S. L., Vauclair, G., Ning, Fu Jian, Chevreton, M., Solheim, J.-E., Gonzalez Perez, J. M., Johannessen, F., Kanaan, A., Costa, J. E. S., Murillo Costa, A. F., Wood, M. A., Silvestri, N., Ahrens, T. J., Jones, A. K., Collins, A. E., Boyer, M., Shaw, J. S., Mukadam, A., Klumpe, E. W., Larrison, J., Kawaler, S., Riddle, R., Ulla, A. and Bradley, P. 2003, A&A, 401, 639

Kuschnig, R., Weiss, W. W., Gruber, R., Bely, P. Y. and Jenkner, H. 1997, A&A, 328, 544

McGraw, J. T., Starrfield, S. G., Liebert, J. and Green, R. F. 1979, in: White dwarfs and variable degenerate stars. (Rochester, NY) 377

Miller Bertolami, M. M. and Althaus, L. G. 2006, A&A, 454, 845

Montgomery, M. H. 2005, ApJ, 633, 1142

Nather, R. E., Winget, D. E., Clemens, J. C., Hansen, C. J. and Hine, B. P. 1990, ApJ, 361, 309

Pesnell, W. D. 1985, ApJ, 292, 238

Pfeiffer, B., Vauclair, G., Dolez, N. et al. 1996, A&A, 314, 182

Press, W. H., Teukolsky, S. A., Vetterling, W. T. and Flannery, B. P. 1996, in *Numerical recipes in FORTRAN: the art of scientific computing*, 2.ed.

Robinson, E. L., Kepler, S. O. and Nather, R. E. 1982, ApJ, 259, 219

Sakurai, J. J. 1994, Modern Quantum Mechanics. Addison-Wesley. ISBN 0-201-53929-2. pp. 104-109.

Scargle, J. D. 1982, ApJ, 263, 835

Schwarzenberg-Czerny, A. 1991, MNRAS, 253, 198

Schwarzenberg-Czerny, A. 1999, MNRAS, 516, 315

Shibahashi, H. 1988, in Advances in Helio and Asteroseismology. IAU Symp. 123, p.133

Sion, E. M., Liebert, J. and Starrfield, S. G. 1985, ApJ, 292, 471

Unno, W., Osaki, Y., Ando, H., Saio, H., Shibahashi, H. 1989 Nonradial Oscillations of Stars, 2nd ed., Univ. Tokyo, Tokyo, p. 378

Vauclair, G., Moskalik, P., Pfeiffer, B., Chevreton, M., Dolez, N., Serre, B., Kleinman, S. J., Barstow, M., Sansom, A. E., Solheim, J.-E., Belmonte, J. A., Kawaler, S. D., Kepler, S. O., Kanaan, A., Giovannini, O., Winget, D. E., Watson, T. K., Nather, R. E., Clemens, J. C., Provencal, J., Dixson, J. S., Yanagida, K., Nitta Kleinman, A., Montgomery, M., Klumpe, E. W., Bruvold, A., O'Brien, M. S., Hansen, C. J., Grauer, A. D., Bradley, P. A., Wood, M. A., Achilleos, N., Jiang, S. Y., Fu, J. N., Marar, T. M. K., Ashoka, B. N., Meistas, E. G., Chernyshev, A. V., Mazeh, T., Leibowitz, E., Hemar, S., Krzezski, J., Pajdosz, G. and Zola, S. 2002, A&A, 381, 122

Vuille, F. 2000, Balt. Ast., 9, 33

Wegner, G., Barry, D. C., Holberg, J. B., Forrester, W. T. and McGraw, J. T. 1982, Bull. A&AS, 14, 914

Weidner, C. and Koester, D. 2003, A&A, 405, 657

Werner, K. 1995, Balt. Ast., 4, 340

Werner, K. and Herwig, F. 2006, PASP, 118, 183

Winget, D.E., Kepler, S.O., Robinson, E.L. and Nather, R.E. 1985, ApJ, 292, 606

Winget, D.E., Nather, R.E., Clemens, J.C., Provencal, J.L., Kleinman, S.J., Bradley, P.A., Wood, M.A., Claver, C.F., Frueh, M.L., Grauer, A.D., Hine, B.P., Hansen, C.J., Fontaine, G., Achilleos, N., Wickramasinghe, D.T., Marar, T.M.K., Seetha, S., Ashoka, B.N., O'Donoghue, D., Warner, B., Kurtz, D.W., Buckley, D.A., Brickhill, J., Vauclair, G., Dolez, N., Chevreton,M., Barstow,M.A., Solheim, J.E., Kanaan, A., Kepler, S.O., Henry, G.W. and Kawaler, S.D. 1991, ApJ, 378, 326 (W91)

[1] Instituto de Física, Universidade Federal do Rio Grande do Sul, 91501-970 Porto Alegre, RS, Brazi — e-mail: costajes@gmail.com

[2] Department of Astronomy & McDonald Observatory, University of Texas, Austin, TX 78712, USA

[3] Gemini Observatory, Hilo, Hawaii, 96720, USA

[4] Department of Physics and Astronomy, Iowa State University, Ames, IA 50011, USA

[5] Universidade de Caxias, Caxias do Sul, RS, Brazil

[6] Departamento de Fíica, Universidade Federal de Santa Catarina, CP 476, CEP 88040-900, Florianópolis, SC, Brazil — e-mail: kanaan@fsc.ufsc.br

[7] Sloan Digital Sky Survey, Apache Pt. Observatory, PO Box 59, Sunspot, NM 88349, USA

[8] Department of Physics and Astronomy, University of Delaware, Newark, DE 19716, USA

[9] Dept. of Physics and Space Sciences & The SARA Observatory, Florida Institute of Technology, Melbourne, FL 32901, USA
[10] Department of Physics and Astronomy, University of Arkansas at Little Rock, USA
[11] Los Alamos National Laboratory, X-2, MS T-085 Los Alamos, NM 87545, USA
[12] Subaru National Astronomical Observatory of Japan, Mitaka, Tokyo 181, Japan — e-mail: kaz@saburu.naoj.org
[13] University of Hawaii, Hilo, Hawaii, USA
[14] Beijing Astronomical Observatory, Academy of Sciences, Beijing 100080, P.R. China — e-mail: jiang@astro.as.utexas.edu
[15] University of Victoria, Wellington, New Zealand
[16] University of North Carolina, Chapell Hill, NC 27599, USA
[17] VU Institute of Theoretical Physics and Astronomy, Goštauto 12, 01108 Vilnius, Lithuania
[18] South African Astronomical Observatory
[19] Mt. Suhora Observatory, Cracow Pedagogical University, UI. Podchorazych 2, 30-084 Cracow, Poland
[20] INAF - Osservatorio Astronomico di Capodimonte, Napoli, Italy
[21] INAF - Osservatorio Astronomico di Bologna, Bologna, Italy
[22] Université Paul Sabatier, Observatoire Midi-Pyrénées, CNRS/UMR5572, 14 av. E. Belin, 31400 Toulouse, France
[23] Observatoire de Paris-Meudon, DAEC, 92195 Meudon, France — e-mail: chevreton@obspm.fr
[24] Institut für Astrophysik,Friedrich-Hund-Platz 1, D-37077 Göttingen, Germany
[25] Institut für Astronomie und Astrophysik Tübingen, Universitat Tübingen, Sand 1, D–72076 Tübingen, Germany
[26] Institutt for Fysikk, Universitetet i Tromsø, N-9037 Tromsø, Norway — e-mail: j.e.solheim@astro.uio.no
[27] Institut for Teoretisk Astrofysikk, Universitetet i Oslo, pb 1029-Blindern, N-0315 Oslo, Norway
[28] Instituto de Astrofisica, C/ Via Lactea s/n, E-38200 La Laguna, Tenerife, Spain
[29] Universidade de Vigo, Depto. de Física Aplicada, Facultade de Ciencias do Mar, Campus Lagoas-Marcosende s/n, 36200 Vigo, Spain
[30] Department of Physics and Astronomy, University of Leicester, UK
[31] High Altitude Observatory, National Center for Atmospheric Research, 3080 Center Green Dr (CG1/3164), USA — e-mail: travis@hao.ucar.edu
[32] Korea Astronomy and Space Science Institute, Daejeon, 305-348, Korea
[33] Terskol Observatory, Ukraine
[34] Ege University Observatory, Bornova 35100, Izmir, Turkey
[35] Konkoly Observatory, P.O. Box 67, H-1525 Budapest, Hungary
[36] Indian Space Research Organization, India
[37] Institut für Astronomie, Universität Wien, Turkenschanzstrasse 17, A-1180 Wien, Austria
[38] Ege University Faculty of Science Astronomy and Space Sciences Department, Izmir, Turkey
[39] Middle Tennessee State University, Department of Physics and Astronomy Murfreesboro, TN 37132, USA
[40] Astronomical Observatory, Jagiellonian University, ul. Orla 171, 30-244 Krakow, Poland — e-mail: szola@oa.uj.edu.pl
[41] Department of Astronomy, The Ohio State University, 140 W. 18th Avenue, Columbus, OH 43210, USA — e-mail: kilic@astronomy.ohio-state.edu
[42] Department of Astronomy, University of Washington, Box 351580, Seattle, WA 98195, USA — e-mail: nms@astro.washington.edu
[43] Instituut voor Sterrenkunde, Celestijnenlaan 200B, 3001 Leuven, Belgium — e-mail: Maja.Vuckovic@ster.kuleuven.be
[44] Thirty Meter Telescope Project, 2632 E. Washington Blvd, Pasadena, CA 91107, USA — e-mail: email: riddle@tmt.org
[45] Facultad de Ciencias Astronómicas y Geofísicas, Universidad Nacional de La Plata, Paseo del Bosque S/N, (1900) La Plata, Argentina — e-mail: althaus@fcaglp.unlp.edu.ar — e-mail: acorsico@fcaglp.unlp.edu.ar
[46] Instituto de Astrofísica La Plata, IALP, CONICET-UNLP, Argentina
[47] Department of Astronomy, Yale University, New Haven, Connecticut, CT 06851, USA — e-mail: obrien@astro.yale.edu
[48] Department of Astronomy, Beijing Normal University, Beijing, P.R.China

Online Material

Table .12. Identified $\ell = 2$ pulsation modes.

$k \pm 2$	m	Period (s)	Freq. (μHz)	Ampl. (mma)	Confid. Level	W91 (ℓ, m)	$k \pm 2$	m	Period (s)	Freq. (μHz)	Ampl. (mma)	Confid. Level	W91 (ℓ, m)
	+1							+1	668.52	1495.84	0.3	5	—
24	0	350.75	2851.03	0.6	3	—	50	0	672.20	1487.65	0.1	5	—
	-1	352.48	2837.04	0.5	5	—		-1					
	-2	353.39	2829.73	0.2	5	—		-2	680.33	1469.88	0.3	3	—
	+1	362.20	2760.91	0.6	3	—		+1					
25	0	363.39	2751.86	0.5	3	2,-2	51	0	684.48	1460.96	0.1	5	—
	-2							-2	693.29	1442.40	0.2		—
	+2							+2	689.77	1449.76	0.5	2	1,-1
	+1							+1	693.29	1442.40	0.2	3	—
26	0	376.03	2659.36	0.3	5	—	52	0	696.83	1435.07	0.4	5	—
	-1	376.65	2654.98	0.7	2	—		-1					
	-2	377.73	2647.29	0.6	3	—		-2	705.80	1416.83	0.7	1	1,+1
	+1	386.93	2584.45	0.4	1	—		+1	705.93	1416.57	0.7	1	1,+1
27	0	387.47	2580.84	0.4	5	2,0	53	0	709.87	1408.71	0.2	5	—
	-1							-1	713.80	1400.95	0.2	5	—
	-2	390.30	2562.13	1.5	1	2,-2		-2					
	+2	397.23	2517.43	0.4	3	—		+2	713.23	1402.07	0.5	3	—
	+1	398.91	2506.83	0.3	2	2,?		+1					
28	0	400.06	2499.63	1.4	1	2,?	54	0					
	-2	402.36	2485.34	0.5	1	—		-2					
	+2	410.43	2436.47	0.7	1	—		+2					
	+1	412.00	2427.18	0.6	1	2,+1:		+1	729.72	1370.39	0.3	5	1,0:
29	0	413.14	2420.49	0.1	5	2,0:	55	0					
	-1	414.37	2413.30	0.6	1	2,-1:		-1					
	-2	415.59	2406.22	1.2	1	2,-2:		-2	742.95	1345.99	0.1	5	—
	+2	422.55	2366.58	2.0	1	2,+2		+2	737.79	1355.40	1.0	1	—
	+1	423.81	2359.55	0.8	1	2,+1		+1					
30	0	425.04	2352.72	0.4	5	2,0	56	0	746.38	1339.80	0.8	1	—
	-1	426.29	2345.82	0.9	1	2,-1		-1					
	-2	427.53	2339.02	1.5	1	2,-2		-2					
	+2	434.96	2299.06	0.1	5	—		+2					
	+1	436.56	2290.64	0.5	1	2,+1		+1					
31	0						57	0					
	-1	439.25	2276.61	0.5	1	2,-1:		-1	763.90	1309.07	0.3	3	—
	-2	440.66	2269.32	0.1	4	2,-2:		-2	768.72	1300.86	0.3	3	—
	+2	446.52	2239.54	0.4	3	—		+2	762.11	1312.15	0.5	3	—
	+1	447.89	2232.69	0.2	5	—		+1					
32	0	449.43	2225.04	0.2	5	—	58	0					
	-1	452.03	2212.24	2.0	1	—		-1	776.63	1287.61	0.3	3	1,-1
	-2	453.26	2206.24	2.0	1	(2),?		-2	780.97	1280.46	0.9	1	—
	+2	458.88	2179.22	0.7	3	—		+2	773.73	1292.44	0.3	3	1,0
	+1	460.71	2170.56	0.3	5	—		+1					
33	0						59	0	783.19	1276.83	0.3	3	—
35	0						60	0					
	-1	488.89	2045.45	0.3	3	—		-1					
	-2							-2	819.95	1219.59	0.8		1,-1
	+2	494.85	2020.81	0.5	1	—		+2					
	+1							+1					
36	0	498.73	2005.09	0.6	1	—	62	0	820.90	1218.18	1.8	1	—
	-1	500.91	1996.37	0.3	3	—		-1					
	+2	507.58	1970.13	0.3	3	—		+2	821.69	1217.00	0.6	3	—
	+1	510.06	1960.55	0.4	3	—		+1					
37	0	511.98	1953.20	0.4	1	—	63	0					
	-1	514.06	1945.30	0.4	3	—		-1	838.65	1192.39	0.6	2	—
	-2	516.03	1937.87	2.0	1	1,+1		-2	844.78	1183.74	0.9	1	—
	+2	519.30	1925.67	0.7	1	—		+2					
	+1							+1					
38	0	524.03	1908.29	0.2	5	—	64	0					
	-1	526.43	1899.59	0.4	1	—		-1					
	-2							-2	857.36	1166.37	0.4	3	—
	+2	531.83	1880.30	1.0	1	—		+2					
	+1							+1	852.08	1173.60	0.6		—
39	0	536.37	1864.38	0.2	5	—	65	0	858.84	1164.36	0.2	4	—
	-2	540.96	1848.57	0.4	1	—		-2					
	+2	544.31	1837.19	0.6	1	—		+2	859.67	1163.24	0.5	3	—
	+1	546.05	1831.33	0.9	1	—		+1					
40	0	547.00	1828.15	0.2	3	—	66	0					
	-1	550.52	1816.46	0.3	3	—		-1	877.10	1140.12	0.3	3	—
	+2	556.64	1796.49	0.3	3	—		+2					
	+1	558.98	1788.97	0.4	3	—		+1					
41	0	561.99	1779.39	0.5	2	—	67	0					
	-1	563.48	1774.68	0.3	3	—		-1	889.67	1124.01	0.4	5	—
	+1	571.19	1750.73	0.5	3	(2),?		+1	901.07	1109.79	0.7	3	—
42	0	573.69	1743.10	1.0	1	—	69	0					
	-1	576.02	1736.05	0.2	5	—		-1					
	-2	579.11	1726.79	0.3	3	2,-1:		-2					
	+2	580.34	1723.13	0.4	3	—		+2					
43	0	585.26	1708.64	0.6	3	—	70	0					
	-2							-2	934.05	1070.61	0.5		2,?
	+1							+1	924.94	1081.15	0.3		—
46	0						71	0					
	-1	626.47	1596.25	0.3	5	—		-1	939.68	1064.19	0.3	5	—

Table .12. continued.

$k \pm 2$	m	Period (s)	Freq. (μHz)	Ampl. (mma)	Confid. Level	W91 (ℓ, m)	$k \pm 2$	m	Period (s)	Freq. (μHz)	Ampl. (mma)	Confid. Level	W91 (ℓ, m)
	-2	629.54	1588.46	0.5	5	—		-2	947.45	1055.46	0.5	1	—
47	0						72	0	945.01	1058.19	0.3	3	—
	-1							-1					
	-2	641.90	1557.88	0.8	3	–		-2					
	+1	644.04	1552.70	0.4	3	—		+1	961.09	1040.49	0.2	5	—
48	0						74	0					
	-1	650.83	1536.50	0.5	3	—		-1					
	+2							+2	966.95	1034.18	0.7		—
49	0	660.46	1514.10	0.4	5	—	75	0	982.68	1017.63	0.2	7	2.?
	-1							-1	988.70	1011.43	0.1		2,-1:
	-2	666.86	1499.57	0.3	3	—		-2					

Table .13. Detected pulsation modes in the 1983 dataset (T_{max} computed from T_o = 244 5346.0 BCT).

Frequency (μHz)	Period (sec)	Amplitude (mma)	T_{max} (s)
1011.9365 ± 0.0079	988.204333 ± 0.007711	1.1791 ± 0.1256	17.62 ± 49.50
1112.6100 ± 0.0111	898.787523 ± 0.008955	0.9190 ± 0.1380	638.41 ± 63.26
1151.0329 ± 0.0119	868.784910 ± 0.008981	0.7887 ± 0.1259	527.90 ± 65.72
1161.1547 ± 0.0101	861.211712 ± 0.007524	0.9217 ± 0.1259	844.50 ± 55.52
1181.1207 ± 0.0090	846.653521 ± 0.006440	1.0447 ± 0.1270	32.58 ± 48.27
1186.4182 ± 0.0046	842.873106 ± 0.003243	2.2830 ± 0.1418	493.04 ± 24.39
1216.9900 ± 0.0160	821.699418 ± 0.010776	0.6305 ± 0.1409	486.90 ± 84.62
1218.1499 ± 0.0053	820.917047 ± 0.003587	1.9605 ± 0.1416	386.19 ± 27.72
1219.8514 ± 0.0073	819.772012 ± 0.004880	1.3999 ± 0.1380	766.46 ± 37.77
1226.9416 ± 0.0099	815.034743 ± 0.006564	1.0191 ± 0.1410	172.52 ± 51.98
1243.3324 ± 0.0141	804.290153 ± 0.009095	0.7829 ± 0.1757	654.30 ± 73.35
1254.5377 ± 0.0133	797.106396 ± 0.008461	0.8206 ± 0.1757	349.41 ± 68.93
1260.5005 ± 0.0119	793.335677 ± 0.007504	0.8284 ± 0.1307	338.19 ± 60.24
1280.4246 ± 0.0109	780.990943 ± 0.006675	0.9026 ± 0.1304	386.32 ± 54.35
1352.4929 ± 0.0170	739.375432 ± 0.009270	0.5584 ± 0.1279	314.78 ± 79.60
1357.6442 ± 0.0107	736.570013 ± 0.005828	0.9506 ± 0.1378	379.29 ± 50.19
1391.4715 ± 0.0134	718.663683 ± 0.006941	0.6877 ± 0.1249	70.92 ± 61.31
1448.5587 ± 0.0148	690.341362 ± 0.007061	0.6323 ± 0.1270	329.19 ± 64.92
1455.0232 ± 0.0092	687.274290 ± 0.004341	1.1181 ± 0.1390	379.94 ± 40.07
1529.1025 ± 0.0108	653.978381 ± 0.004640	0.8726 ± 0.1285	292.69 ± 45.02
1535.1914 ± 0.0202	651.384588 ± 0.008592	0.4664 ± 0.1278	327.07 ± 83.68
1611.2702 ± 0.0107	620.628356 ± 0.004117	0.9618 ± 0.1389	465.32 ± 42.10
1700.9494 ± 0.0157	587.906960 ± 0.005411	0.6505 ± 0.1376	421.02 ± 58.42
1755.9298 ± 0.0198	569.498851 ± 0.006418	0.5359 ± 0.1432	64.88 ± 71.52
1764.1313 ± 0.0116	566.851230 ± 0.003729	0.9206 ± 0.1446	359.75 ± 41.72
1779.4498 ± 0.0090	561.971446 ± 0.002833	1.2115 ± 0.1473	412.12 ± 31.99
1809.1382 ± 0.0178	552.749380 ± 0.005437	0.6271 ± 0.1496	526.53 ± 62.80
1823.7553 ± 0.0113	548.319169 ± 0.003389	0.9871 ± 0.1492	495.74 ± 39.35
1829.6743 ± 0.0135	546.545366 ± 0.004023	0.7892 ± 0.1433	234.94 ± 46.77
1854.0516 ± 0.0021	539.359305 ± 0.000601	5.9342 ± 0.1617	532.55 ± 7.14
1858.1887 ± 0.0027	538.158481 ± 0.000793	4.4800 ± 0.1618	140.06 ± 9.44
1862.7482 ± 0.0106	536.841215 ± 0.003062	1.0068 ± 0.1447	51.93 ± 36.17
1877.5834 ± 0.0193	532.599526 ± 0.005468	0.5525 ± 0.1444	413.36 ± 65.14
1901.2433 ± 0.0099	525.971619 ± 0.002744	1.1041 ± 0.1462	482.25 ± 33.19
1928.0004 ± 0.0141	518.672104 ± 0.003794	0.6720 ± 0.1285	359.36 ± 46.42
1932.6317 ± 0.0088	517.429174 ± 0.002354	1.2554 ± 0.1492	274.07 ± 28.90
1933.7778 ± 0.0085	517.122487 ± 0.002267	1.3028 ± 0.1473	499.16 ± 27.89
1937.8870 ± 0.0013	516.025972 ± 0.000359	8.7643 ± 0.1604	223.87 ± 4.42
1941.4769 ± 0.0117	515.071793 ± 0.003093	0.9146 ± 0.1442	156.07 ± 38.11
1963.7950 ± 0.0164	509.218114 ± 0.004257	0.5715 ± 0.1269	218.49 ± 53.05
2005.9249 ± 0.0159	498.523151 ± 0.003947	0.6724 ± 0.1444	409.06 ± 50.25
2006.4344 ± 0.0145	498.396553 ± 0.003601	0.7311 ± 0.1429	255.65 ± 45.92
2020.5927 ± 0.0047	494.904296 ± 0.001156	2.3447 ± 0.1491	3.71 ± 14.83
2025.2590 ± 0.0022	493.764000 ± 0.000527	5.4731 ± 0.1600	182.52 ± 6.78
2026.0712 ± 0.0095	493.566068 ± 0.002309	1.1630 ± 0.1476	313.03 ± 29.76
2029.6308 ± 0.0244	492.700450 ± 0.005930	0.3990 ± 0.1330	115.65 ± 76.54
2051.9225 ± 0.0119	487.347832 ± 0.002833	0.8185 ± 0.1320	321.17 ± 36.91
2072.0988 ± 0.0149	482.602478 ± 0.003471	0.6545 ± 0.1332	170.74 ± 45.76
2087.8452 ± 0.0110	478.962716 ± 0.002533	0.8871 ± 0.1326	309.38 ± 33.55
2119.5632 ± 0.0125	471.795314 ± 0.002781	0.7708 ± 0.1301	20.26 ± 37.44
2128.4479 ± 0.0152	469.825928 ± 0.003348	0.6276 ± 0.1293	153.32 ± 45.21
2133.1093 ± 0.0109	468.799230 ± 0.002404	0.9720 ± 0.1438	118.38 ± 32.56
2141.8612 ± 0.0138	466.883655 ± 0.003019	0.7126 ± 0.1336	296.95 ± 41.04
2171.5971 ± 0.0126	460.490575 ± 0.002680	0.7510 ± 0.1284	124.18 ± 36.93
2177.4422 ± 0.0079	459.254450 ± 0.001671	1.3725 ± 0.1472	352.71 ± 23.09
2178.4015 ± 0.0110	459.052210 ± 0.002324	0.8789 ± 0.1314	424.17 ± 32.15
2206.2713 ± 0.0076	453.253413 ± 0.001554	1.4114 ± 0.1444	79.20 ± 21.76
2210.2990 ± 0.0041	452.427481 ± 0.000838	2.7826 ± 0.1520	75.60 ± 11.74
2212.5858 ± 0.0162	451.959885 ± 0.003305	0.5801 ± 0.1270	289.54 ± 46.42
2214.3841 ± 0.0025	451.592837 ± 0.000511	4.5395 ± 0.1519	345.00 ± 7.16
2222.8546 ± 0.0115	449.871985 ± 0.002336	0.9125 ± 0.1429	251.75 ± 32.95
2249.1975 ± 0.0077	444.603024 ± 0.001515	1.4051 ± 0.1457	56.58 ± 21.63
2259.0124 ± 0.0159	442.671322 ± 0.003109	0.6013 ± 0.1293	151.59 ± 44.58
2273.3189 ± 0.0115	439.885501 ± 0.002218	0.9272 ± 0.1437	37.27 ± 32.03
2316.7935 ± 0.0105	431.631037 ± 0.001953	0.9266 ± 0.1316	377.13 ± 28.75
2324.3126 ± 0.0171	430.234724 ± 0.003171	0.6123 ± 0.1404	148.06 ± 46.68
2334.7293 ± 0.0076	428.315172 ± 0.001394	1.2879 ± 0.1326	416.39 ± 20.64
2336.4100 ± 0.0115	428.007074 ± 0.002113	0.9080 ± 0.1405	333.24 ± 31.25
2340.6038 ± 0.0120	427.240179 ± 0.002185	0.7996 ± 0.1297	177.87 ± 32.45
2366.6416 ± 0.0042	422.539691 ± 0.000754	2.3616 ± 0.1349	81.13 ± 11.33
2369.4702 ± 0.0084	422.035264 ± 0.001491	1.1572 ± 0.1303	327.43 ± 22.43
2383.2251 ± 0.0059	419.599475 ± 0.001035	1.6882 ± 0.1337	219.72 ± 15.66
2401.8652 ± 0.0167	416.343105 ± 0.002891	0.5787 ± 0.1302	389.12 ± 44.08
2415.2562 ± 0.0100	414.034745 ± 0.001713	0.9684 ± 0.1305	266.36 ± 26.27
2436.4093 ± 0.0134	410.440061 ± 0.002252	0.7345 ± 0.1315	354.62 ± 34.89
2462.0764 ± 0.0153	406.161236 ± 0.002524	0.6309 ± 0.1300	97.49 ± 39.44
2512.4785 ± 0.0170	398.013362 ± 0.002691	0.5859 ± 0.1339	397.56 ± 42.92
2522.7090 ± 0.0167	396.399270 ± 0.002632	0.5855 ± 0.1312	364.67 ± 42.21
2562.2870 ± 0.0056	390.276339 ± 0.000856	1.7742 ± 0.1349	243.50 ± 13.92
2597.5527 ± 0.0218	384.977754 ± 0.003231	0.4413 ± 0.1302	247.21 ± 53.27
2640.8545 ± 0.0144	378.665322 ± 0.002058	0.6903 ± 0.1338	30.95 ± 34.49
2655.0047 ± 0.0136	376.647173 ± 0.001929	0.7176 ± 0.1319	376.05 ± 32.52
2684.9228 ± 0.0144	372.450192 ± 0.001996	0.6832 ± 0.1328	337.22 ± 34.03

Table .13. continued.

Frequency (μHz)	Period (sec)	Amplitude (mma)	T_{max} (s)
2700.0979 ± 0.0215	370.356941 ± 0.002946	0.4454 ± 0.1296	146.36 ± 50.48
2760.8020 ± 0.0175	362.213595 ± 0.002299	0.5611 ± 0.1328	201.08 ± 40.31
2837.1015 ± 0.0175	352.472408 ± 0.002172	0.5425 ± 0.1285	252.36 ± 39.09

Table .14. Detected pulsation modes in the 1985 dataset (T_{max} computed from T_o = 244 6147.0 BCT).

Frequency (μHz)	Period (sec)	Amplitude (mma)	T_{max} [2] (s)
1034.5428 ± 0.0217	966.610560 ± 0.020314	0.6849 ± 0.1988	736.76 ± 94.62
1078.0905 ± 0.0201	927.565918 ± 0.017289	0.6848 ± 0.1815	516.68 ± 84.53
1102.9193 ± 0.0235	906.684649 ± 0.019318	0.5980 ± 0.1865	336.53 ± 95.88
1135.4811 ± 0.0212	880.683988 ± 0.016460	0.6612 ± 0.1822	742.20 ± 86.97
1160.5270 ± 0.0124	861.677505 ± 0.009235	1.0889 ± 0.1814	189.62 ± 48.88
1160.6326 ± 0.0089	861.599096 ± 0.006592	1.5447 ± 0.1821	226.99 ± 34.68
1167.8772 ± 0.0206	856.254435 ± 0.015102	0.6882 ± 0.1837	715.95 ± 82.30
1173.5780 ± 0.0201	852.095023 ± 0.014619	0.6553 ± 0.1746	417.38 ± 77.38
1186.6776 ± 0.0131	842.688835 ± 0.009292	1.0753 ± 0.1868	595.48 ± 49.73
1230.8545 ± 0.0187	812.443695 ± 0.012359	0.7349 ± 0.1812	196.48 ± 69.76
1265.0999 ± 0.0260	790.451391 ± 0.016224	0.7356 ± 0.2509	378.00 ± 98.51
1265.3800 ± 0.0108	790.276444 ± 0.006735	1.3816 ± 0.1988	351.40 ± 38.37
1274.6813 ± 0.0261	784.509853 ± 0.016070	0.7337 ± 0.2510	224.14 ± 98.27
1339.7982 ± 0.0155	746.381081 ± 0.008647	0.8750 ± 0.1805	7.76 ± 52.24
1402.0384 ± 0.0247	713.247214 ± 0.012565	0.5407 ± 0.1777	292.46 ± 79.40
1416.7367 ± 0.0189	705.847439 ± 0.009436	0.7605 ± 0.1919	161.39 ± 60.26
1446.1612 ± 0.0158	691.485856 ± 0.007577	0.9403 ± 0.1985	635.83 ± 49.36
1471.8909 ± 0.0243	679.398170 ± 0.011201	0.5597 ± 0.1807	185.42 ± 74.34
1475.5162 ± 0.0290	677.728912 ± 0.013319	0.4697 ± 0.1795	240.86 ± 89.38
1550.6392 ± 0.0104	644.895333 ± 0.004318	1.7487 ± 0.2415	86.68 ± 30.18
1584.5568 ± 0.0198	631.091302 ± 0.007887	0.7024 ± 0.1772	552.05 ± 57.01
1588.4141 ± 0.0255	629.558741 ± 0.010126	0.5431 ± 0.1761	478.52 ± 73.22
1617.4207 ± 0.0278	618.268316 ± 0.010612	0.4886 ± 0.1806	466.49 ± 77.32
1619.9864 ± 0.0178	617.289125 ± 0.006780	0.8086 ± 0.1921	206.64 ± 49.57
1717.5117 ± 0.0373	582.237654 ± 0.012652	0.3535 ± 0.1772	181.18 ± 97.57
1718.2909 ± 0.0284	581.973646 ± 0.009610	0.5009 ± 0.1888	77.54 ± 74.76
1743.0959 ± 0.0135	573.691892 ± 0.004453	1.0035 ± 0.1809	86.98 ± 35.00
1763.4590 ± 0.0268	567.067343 ± 0.008618	0.4986 ± 0.1781	467.81 ± 68.63
1780.7922 ± 0.0130	561.547822 ± 0.004095	1.0315 ± 0.1798	307.14 ± 32.91
1790.2400 ± 0.0252	558.584319 ± 0.007858	0.5249 ± 0.1782	131.33 ± 63.25
1800.4563 ± 0.0139	555.414752 ± 0.004286	1.0264 ± 0.1885	189.10 ± 34.92
1807.1851 ± 0.0253	553.346743 ± 0.007737	0.5230 ± 0.1784	302.81 ± 62.89
1823.6754 ± 0.0108	548.343187 ± 0.003262	1.3674 ± 0.1927	292.15 ± 27.08
1826.2281 ± 0.0179	547.576729 ± 0.005362	0.7463 ± 0.1748	128.89 ± 44.42
1853.9013 ± 0.0033	539.403043 ± 0.000971	4.4803 ± 0.1985	430.19 ± 8.12
1858.2488 ± 0.0033	538.141067 ± 0.000959	4.8752 ± 0.2149	131.71 ± 8.03
1893.5625 ± 0.0131	528.105086 ± 0.003655	1.1711 ± 0.1998	352.02 ± 31.27
1911.4126 ± 0.0160	523.173287 ± 0.004367	0.8856 ± 0.1879	380.39 ± 37.72
1933.7114 ± 0.0054	517.140243 ± 0.001440	3.0092 ± 0.2152	485.22 ± 12.55
1937.8440 ± 0.0024	516.037412 ± 0.000650	7.4480 ± 0.2414	28.37 ± 5.68
1941.6301 ± 0.0123	515.031147 ± 0.003263	1.2133 ± 0.1991	387.92 ± 28.38
1967.5851 ± 0.0217	508.237238 ± 0.005617	0.6510 ± 0.1824	480.79 ± 50.88
2005.0693 ± 0.0112	498.735878 ± 0.002793	1.3306 ± 0.1987	81.86 ± 25.24
2020.9467 ± 0.0121	494.817607 ± 0.002974	1.1327 ± 0.1808	93.61 ± 27.12
2025.3204 ± 0.0054	493.749041 ± 0.001320	2.9996 ± 0.2154	290.75 ± 12.07
2064.3576 ± 0.0122	484.412195 ± 0.002853	1.1559 ± 0.1871	147.21 ± 26.56
2103.2286 ± 0.0176	475.459501 ± 0.003969	0.7866 ± 0.1817	216.98 ± 37.66
2176.4901 ± 0.0128	459.455332 ± 0.002696	1.1370 ± 0.1942	431.99 ± 26.61
2179.1563 ± 0.0196	458.893196 ± 0.004136	0.7141 ± 0.1872	346.20 ± 40.61
2195.4017 ± 0.0292	455.497513 ± 0.006050	0.4674 ± 0.1814	312.52 ± 59.94
2210.5733 ± 0.0109	452.371342 ± 0.002224	1.3724 ± 0.1986	143.63 ± 22.16
2214.4590 ± 0.0060	451.577571 ± 0.001213	2.7234 ± 0.2149	308.42 ± 12.13
2219.4165 ± 0.0123	450.568874 ± 0.002497	1.1831 ± 0.1943	323.79 ± 25.16
2219.5751 ± 0.0058	450.536692 ± 0.001180	3.1264 ± 0.2419	44.14 ± 11.81
2269.4384 ± 0.0189	440.637642 ± 0.003674	0.6945 ± 0.1754	338.86 ± 37.59
2302.3939 ± 0.0160	434.330549 ± 0.003024	0.8768 ± 0.1869	306.06 ± 31.42
2331.3456 ± 0.0354	428.936832 ± 0.006513	0.4683 ± 0.2034	409.67 ± 68.48
2334.0609 ± 0.0108	428.437841 ± 0.001982	1.2824 ± 0.1813	65.21 ± 20.93
2354.4629 ± 0.0461	424.725320 ± 0.008317	0.3600 ± 0.2032	46.07 ± 88.33
2364.9175 ± 0.0198	422.847741 ± 0.003540	0.6717 ± 0.1771	49.45 ± 37.74
2371.2417 ± 0.0103	421.719989 ± 0.001832	1.4474 ± 0.1986	260.20 ± 19.58
2389.6684 ± 0.0109	418.468103 ± 0.001911	1.4818 ± 0.2150	218.43 ± 20.59
2407.1592 ± 0.0171	415.427442 ± 0.002959	0.8055 ± 0.1809	30.17 ± 32.22
2433.7686 ± 0.0149	410.885402 ± 0.002517	0.9678 ± 0.1914	195.63 ± 27.65
2439.2207 ± 0.0131	409.967002 ± 0.002198	1.0734 ± 0.1868	73.11 ± 24.18
2511.8868 ± 0.0261	398.107114 ± 0.004131	0.5253 ± 0.1749	231.33 ± 47.30
2517.4640 ± 0.0267	397.225150 ± 0.004212	0.4874 ± 0.1734	374.09 ± 47.73
2562.3537 ± 0.0135	390.266188 ± 0.002054	1.1989 ± 0.2149	175.43 ± 23.71
2584.3824 ± 0.0304	386.939638 ± 0.004556	0.4486 ± 0.1752	380.99 ± 53.65
2605.7493 ± 0.0241	383.766768 ± 0.003543	0.6205 ± 0.1995	144.87 ± 41.66
2654.4085 ± 0.0235	376.731762 ± 0.003330	0.6139 ± 0.1913	150.64 ± 39.87
2659.2838 ± 0.0402	376.041099 ± 0.005684	0.3491 ± 0.1871	269.52 ± 68.11
2717.2780 ± 0.0238	368.015347 ± 0.003220	0.6278 ± 0.1993	90.92 ± 39.46
2773.3897 ± 0.0482	360.569597 ± 0.006269	0.3378 ± 0.1764	227.32 ± 82.35
2775.9713 ± 0.0459	360.234271 ± 0.005954	0.3546 ± 0.1762	147.01 ± 78.27
2786.2589 ± 0.0308	358.904199 ± 0.003964	0.4555 ± 0.1867	277.29 ± 49.77
2851.0184 ± 0.0275	350.751857 ± 0.003387	0.5890 ± 0.2152	199.07 ± 43.54
2903.0088 ± 0.0634	344.470198 ± 0.007524	0.2267 ± 0.1912	181.87 ± 98.45
2972.3323 ± 0.0278	336.436139 ± 0.003150	0.5829 ± 0.2150	191.96 ± 42.22

Table .15. Detected pulsation modes in the 1989 dataset (T_{max} computed from T_o = 244 7593.0 BCT). .

Frequency (μHz)	Period (sec)	Amplitude (mma)	T_{max} (s)
1017.6244 ± 0.1505	982.680884 ± 0.145369	0.2355 ± 0.0527	835.02 ± 83.61
1081.1478 ± 0.1171	924.942960 ± 0.100212	0.2865 ± 0.0518	685.45 ± 61.49
1083.0795 ± 0.0576	923.293233 ± 0.049073	0.5750 ± 0.0519	578.15 ± 30.48
1155.9663 ± 0.1244	865.077117 ± 0.093109	0.2678 ± 0.0522	49.06 ± 62.12
1164.3414 ± 0.1462	858.854597 ± 0.107846	0.2277 ± 0.0523	183.33 ± 72.72
1186.3982 ± 0.0364	842.887344 ± 0.025827	0.9129 ± 0.0520	621.86 ± 17.59
1194.5258 ± 0.0694	837.152258 ± 0.048667	0.4734 ± 0.0514	413.69 ± 33.26
1219.5889 ± 0.0412	819.948424 ± 0.027698	0.8064 ± 0.0526	736.66 ± 19.47
1223.4084 ± 0.1365	817.388508 ± 0.091173	0.2412 ± 0.0514	121.26 ± 63.84
1227.6156 ± 0.0757	814.587257 ± 0.050229	0.4336 ± 0.0514	645.39 ± 35.33
1230.6595 ± 0.0814	812.572474 ± 0.053740	0.4082 ± 0.0526	308.64 ± 38.12
1276.8218 ± 0.1238	783.194636 ± 0.075956	0.2729 ± 0.0522	447.87 ± 55.98
1287.5897 ± 0.0941	776.644911 ± 0.056747	0.3601 ± 0.0521	216.57 ± 42.35
1292.4168 ± 0.1075	773.744170 ± 0.064379	0.3091 ± 0.0515	256.44 ± 47.87
1300.8603 ± 0.1254	768.722034 ± 0.074088	0.2620 ± 0.0514	109.60 ± 55.25
1323.8489 ± 0.1114	755.373222 ± 0.063550	0.3060 ± 0.0523	522.84 ± 47.98
1345.9740 ± 0.2271	742.956428 ± 0.125357	0.1515 ± 0.0529	498.10 ± 95.94
1359.3972 ± 0.2012	735.620174 ± 0.108857	0.1695 ± 0.0540	610.86 ± 83.76
1365.8060 ± 0.1254	732.168389 ± 0.067237	0.2618 ± 0.0514	72.66 ± 52.63
1367.1423 ± 0.0350	731.452732 ± 0.018711	0.9771 ± 0.0524	711.78 ± 14.87
1370.8007 ± 0.1154	729.500659 ± 0.061392	0.2903 ± 0.0526	237.90 ± 48.05
1373.6916 ± 0.1595	727.965433 ± 0.084543	0.2100 ± 0.0523	251.61 ± 66.06
1375.3251 ± 0.0473	727.100800 ± 0.025032	0.7227 ± 0.0524	5.58 ± 19.98
1416.5690 ± 0.0441	705.931037 ± 0.021974	0.7513 ± 0.0519	314.76 ± 17.84
1442.3849 ± 0.1604	693.296238 ± 0.077092	0.2145 ± 0.0523	614.41 ± 64.41
1449.7783 ± 0.0676	689.760631 ± 0.032140	0.5101 ± 0.0521	157.26 ± 26.92
1454.0459 ± 0.0900	687.736194 ± 0.042572	0.3689 ± 0.0524	587.77 ± 35.55
1458.1900 ± 0.1912	685.781680 ± 0.089917	0.1725 ± 0.0514	340.92 ± 75.00
1487.6353 ± 0.2375	672.207780 ± 0.107307	0.1438 ± 0.0536	21.18 ± 91.14
1495.7875 ± 0.0999	668.544150 ± 0.044649	0.3496 ± 0.0547	535.93 ± 38.06
1496.8471 ± 0.0556	668.070922 ± 0.024808	0.5948 ± 0.0515	417.71 ± 21.26
1499.5242 ± 0.1066	666.878186 ± 0.047388	0.3122 ± 0.0522	524.33 ± 40.83
1505.0529 ± 0.1092	664.428487 ± 0.048187	0.3120 ± 0.0529	387.82 ± 41.10
1550.4193 ± 0.0396	644.986828 ± 0.016481	0.8661 ± 0.0532	47.76 ± 14.54
1554.4871 ± 0.0614	643.298997 ± 0.025423	0.5349 ± 0.0515	509.52 ± 22.66
1558.7631 ± 0.0334	641.534310 ± 0.013752	1.0265 ± 0.0533	553.31 ± 12.20
1719.1686 ± 0.0339	581.676519 ± 0.011483	0.9750 ± 0.0519	0.77 ± 11.31
1726.7450 ± 0.1159	579.124301 ± 0.038885	0.2812 ± 0.0511	26.09 ± 38.52
1786.6284 ± 0.0396	559.713468 ± 0.012405	0.8354 ± 0.0519	197.14 ± 12.71
1790.6783 ± 0.0139	558.447616 ± 0.004335	2.4897 ± 0.0545	275.26 ± 4.46
1794.8854 ± 0.0111	557.138625 ± 0.003434	3.1440 ± 0.0546	135.76 ± 3.54
1804.0014 ± 0.1315	554.323292 ± 0.040413	0.2488 ± 0.0512	16.04 ± 41.71
1824.8078 ± 0.2048	548.002915 ± 0.061511	0.1593 ± 0.0513	293.96 ± 64.32
1854.0658 ± 0.0068	539.355194 ± 0.001982	5.3727 ± 0.0564	392.63 ± 2.10
1858.2018 ± 0.0091	538.154698 ± 0.002640	3.8176 ± 0.0548	173.63 ± 2.83
1862.3605 ± 0.0260	536.952969 ± 0.007486	1.4123 ± 0.0563	322.28 ± 7.97
1899.8434 ± 0.2042	526.359180 ± 0.056574	0.1600 ± 0.0512	353.43 ± 61.65
1929.4276 ± 0.0103	518.288425 ± 0.002764	3.5757 ± 0.0562	60.53 ± 3.05
1933.6139 ± 0.0089	517.166333 ± 0.002383	3.8907 ± 0.0548	414.10 ± 2.65
1937.7787 ± 0.0060	516.054807 ± 0.001586	6.1725 ± 0.0562	15.74 ± 1.76
1953.1183 ± 0.1119	512.001750 ± 0.029321	0.2939 ± 0.0512	192.75 ± 32.84
1957.9498 ± 0.1110	510.738317 ± 0.028949	0.2960 ± 0.0513	167.15 ± 32.55
1994.3999 ± 0.1183	501.403964 ± 0.029750	0.2910 ± 0.0537	499.42 ± 33.86
1996.3986 ± 0.1183	500.901973 ± 0.029689	0.2761 ± 0.0511	343.39 ± 34.00
2005.0984 ± 0.0683	498.728633 ± 0.016994	0.5148 ± 0.0538	253.86 ± 19.45
2016.1480 ± 0.1777	495.995325 ± 0.043722	0.1959 ± 0.0539	391.98 ± 50.50
2020.7602 ± 0.0728	494.863279 ± 0.017839	0.4635 ± 0.0525	276.16 ± 20.54
2025.1181 ± 0.0099	493.798373 ± 0.002425	3.4706 ± 0.0541	451.15 ± 2.82
2033.1382 ± 0.1143	491.850489 ± 0.027658	0.2931 ± 0.0521	452.71 ± 32.04
2206.3680 ± 0.0492	453.233543 ± 0.010101	0.6726 ± 0.0519	306.31 ± 12.79
2210.2818 ± 0.0103	452.431007 ± 0.002103	3.3597 ± 0.0544	288.90 ± 2.68
2212.1173 ± 0.0916	452.055590 ± 0.018725	0.3552 ± 0.0510	145.16 ± 23.77
2214.3950 ± 0.0093	451.590617 ± 0.001906	3.6952 ± 0.0544	112.64 ± 2.43
2269.1586 ± 0.0316	440.691991 ± 0.006138	1.0518 ± 0.0521	54.68 ± 8.00
2276.4452 ± 0.0695	439.281377 ± 0.013402	0.4861 ± 0.0528	387.34 ± 17.33
2290.8154 ± 0.0842	436.525798 ± 0.016050	0.4088 ± 0.0523	181.89 ± 20.83
2328.2752 ± 0.0938	429.502487 ± 0.017313	0.3710 ± 0.0539	237.35 ± 23.03
2338.8610 ± 0.0181	427.558544 ± 0.003300	1.9225 ± 0.0539	202.62 ± 4.42
2345.4819 ± 0.1009	426.351623 ± 0.018341	0.3333 ± 0.0519	415.13 ± 24.80
2352.7107 ± 0.0825	425.041635 ± 0.014898	0.4074 ± 0.0519	409.23 ± 20.20
2366.7507 ± 0.0436	422.520217 ± 0.007785	0.7702 ± 0.0525	14.13 ± 10.51
2404.1168 ± 0.0894	415.953171 ± 0.015460	0.3869 ± 0.0536	409.35 ± 21.31
2406.1507 ± 0.0287	415.601567 ± 0.004960	1.1933 ± 0.0527	82.93 ± 6.87
2408.5641 ± 0.2037	415.185136 ± 0.035118	0.1609 ± 0.0513	151.70 ± 48.51
2413.1890 ± 0.0542	414.389421 ± 0.009312	0.6461 ± 0.0539	62.29 ± 12.94
2420.4775 ± 0.1766	413.141629 ± 0.030138	0.1854 ± 0.0513	137.51 ± 41.84
2427.1272 ± 0.0547	412.009726 ± 0.009277	0.6025 ± 0.0515	123.19 ± 12.90
2485.0991 ± 0.1152	402.398437 ± 0.018661	0.2825 ± 0.0510	91.61 ± 26.60
2499.6344 ± 0.0241	400.058512 ± 0.003859	1.4193 ± 0.0532	69.66 ± 5.53
2506.8053 ± 0.0880	398.914115 ± 0.013999	0.3728 ± 0.0514	272.35 ± 20.13
2562.1587 ± 0.0329	390.295893 ± 0.005015	1.0058 ± 0.0519	269.36 ± 7.37
2580.6640 ± 0.1095	387.497178 ± 0.016437	0.2971 ± 0.0510	156.59 ± 24.35

Table .16. Detected pulsation modes in the 1993 dataset (T_{max} computed from T_o = 244 6147.0 BCT).

Frequency (μHz)	Period (sec)	Amplitude (mma)	T_{max} (s)
1033.2862 ± 0.0900	967.786090 ± 0.084282	0.3132 ± 0.0709	941.51 ± 64.90
1034.1774 ± 0.0382	966.952057 ± 0.035763	0.7283 ± 0.0700	156.13 ± 27.45
1039.2650 ± 0.0916	962.218468 ± 0.084791	0.3065 ± 0.0709	729.29 ± 65.82
1058.2071 ± 0.0793	944.994582 ± 0.070789	0.3558 ± 0.0701	272.82 ± 55.76
1080.2204 ± 0.0870	925.737038 ± 0.074575	0.3189 ± 0.0697	897.77 ± 59.84
1139.4529 ± 0.0912	877.614173 ± 0.070280	0.3044 ± 0.0697	254.65 ± 59.55
1140.1251 ± 0.0981	877.096766 ± 0.075488	0.2824 ± 0.0695	37.96 ± 63.94
1160.2915 ± 0.0395	861.852395 ± 0.029347	0.7204 ± 0.0709	686.17 ± 25.33
1163.2534 ± 0.0501	859.657957 ± 0.037026	0.5567 ± 0.0701	808.54 ± 31.95
1166.3591 ± 0.0735	857.368871 ± 0.054024	0.4417 ± 0.0723	197.67 ± 47.40
1167.3995 ± 0.0511	856.604768 ± 0.037496	0.6338 ± 0.0714	438.91 ± 32.65
1171.6597 ± 0.0896	853.490112 ± 0.065293	0.3129 ± 0.0702	586.99 ± 56.99
1192.4088 ± 0.0450	838.638565 ± 0.031625	0.6224 ± 0.0702	220.03 ± 28.11
1197.1341 ± 0.0983	835.328307 ± 0.068583	0.2826 ± 0.0697	144.95 ± 60.98
1220.1689 ± 0.0430	819.558646 ± 0.028858	0.6508 ± 0.0701	552.22 ± 26.15
1309.0639 ± 0.0807	763.904662 ± 0.047121	0.3677 ± 0.0726	217.47 ± 45.58
1314.8173 ± 0.0994	760.561941 ± 0.057486	0.2815 ± 0.0699	186.80 ± 56.28
1320.4297 ± 0.1316	757.329209 ± 0.075477	0.2261 ± 0.0771	711.09 ± 74.84
1324.0973 ± 0.0857	755.231490 ± 0.048879	0.3268 ± 0.0700	333.45 ± 48.18
1332.3277 ± 0.0178	750.566122 ± 0.010052	1.6315 ± 0.0780	501.89 ± 10.08
1344.2132 ± 0.1346	743.929621 ± 0.074506	0.2142 ± 0.0745	184.53 ± 75.63
1366.8532 ± 0.0523	731.607465 ± 0.028017	0.5452 ± 0.0704	176.88 ± 28.58
1370.3877 ± 0.0768	729.720507 ± 0.040906	0.3614 ± 0.0698	138.18 ± 41.62
1389.6408 ± 0.0719	719.610424 ± 0.037228	0.3991 ± 0.0707	333.50 ± 38.71
1400.9626 ± 0.1245	713.794935 ± 0.063452	0.2251 ± 0.0699	229.35 ± 65.67
1408.7119 ± 0.1060	709.868381 ± 0.053430	0.2643 ± 0.0698	269.36 ± 55.65
1410.3156 ± 0.0759	709.061159 ± 0.038169	0.3700 ± 0.0703	468.66 ± 40.06
1437.1959 ± 0.1182	695.799355 ± 0.057216	0.2440 ± 0.0713	45.98 ± 61.72
1449.6613 ± 0.0492	689.816324 ± 0.023429	0.6045 ± 0.0708	88.77 ± 24.74
1458.0250 ± 0.0717	685.859316 ± 0.033749	0.3936 ± 0.0709	256.25 ± 36.73
1460.8938 ± 0.1669	684.512460 ± 0.078199	0.1779 ± 0.0716	490.11 ± 84.06
1469.9053 ± 0.0962	680.315961 ± 0.044504	0.2948 ± 0.0711	446.71 ± 48.71
1474.0148 ± 0.1176	678.419251 ± 0.054138	0.2410 ± 0.0711	85.46 ± 59.29
1537.7154 ± 0.0856	650.315397 ± 0.036210	0.3291 ± 0.0697	455.33 ± 41.56
1552.6555 ± 0.0727	644.057891 ± 0.030169	0.3895 ± 0.0700	436.86 ± 34.65
1559.0218 ± 0.0801	641.427846 ± 0.032940	0.3544 ± 0.0700	225.65 ± 38.03
1607.6603 ± 0.0827	622.021937 ± 0.031990	0.3365 ± 0.0698	338.49 ± 38.21
1723.1638 ± 0.0566	580.327893 ± 0.019058	0.4983 ± 0.0716	387.76 ± 24.44
1736.0197 ± 0.1180	576.030323 ± 0.039138	0.2388 ± 0.0709	321.35 ± 51.08
1774.7121 ± 0.0795	563.471691 ± 0.025253	0.3791 ± 0.0768	509.13 ± 33.46
1779.3249 ± 0.0717	562.010920 ± 0.022644	0.4311 ± 0.0775	343.25 ± 29.57
1786.4773 ± 0.0250	559.760815 ± 0.007836	1.3773 ± 0.0781	283.92 ± 10.60
1787.6437 ± 0.0881	559.395583 ± 0.027580	0.3756 ± 0.0763	414.67 ± 37.91
1788.9755 ± 0.0786	558.979164 ± 0.024561	0.3969 ± 0.0765	374.54 ± 33.25
1790.6871 ± 0.0233	558.444856 ± 0.007271	1.5092 ± 0.0840	52.03 ± 9.39
1794.9656 ± 0.0443	557.113746 ± 0.013750	0.6912 ± 0.0755	313.15 ± 18.52
1796.4485 ± 0.0803	556.653867 ± 0.024878	0.3801 ± 0.0746	271.90 ± 33.10
1802.5758 ± 0.2227	554.761699 ± 0.068546	0.1424 ± 0.0772	9.31 ± 88.33
1816.4675 ± 0.0899	550.519073 ± 0.027252	0.3188 ± 0.0711	380.79 ± 36.83
1837.1351 ± 0.0689	544.325793 ± 0.020423	0.4111 ± 0.0699	360.34 ± 27.97
1842.7054 ± 0.1386	542.680350 ± 0.040818	0.2191 ± 0.0741	68.66 ± 55.07
1848.5585 ± 0.0511	540.962043 ± 0.014962	0.5506 ± 0.0705	385.61 ± 20.58
1854.0679 ± 0.0041	539.354562 ± 0.001199	7.4667 ± 0.0780	272.24 ± 1.65
1858.1632 ± 0.0104	538.165870 ± 0.003017	2.8177 ± 0.0732	93.17 ± 4.21
1859.8665 ± 0.0614	537.672989 ± 0.017757	0.4629 ± 0.0701	453.52 ± 24.57
1862.2440 ± 0.0238	536.986550 ± 0.006872	1.1779 ± 0.0703	130.11 ± 9.50
1862.8139 ± 0.0539	536.822283 ± 0.015526	0.5164 ± 0.0698	427.05 ± 21.49
1864.3898 ± 0.1090	536.368511 ± 0.031348	0.2625 ± 0.0707	416.62 ± 43.72
1866.0015 ± 0.2279	535.905253 ± 0.065441	0.1287 ± 0.0754	403.22 ± 92.13
1866.8473 ± 0.1130	535.662450 ± 0.032423	0.2520 ± 0.0705	492.49 ± 45.25
1889.2619 ± 0.0808	529.307254 ± 0.022637	0.3493 ± 0.0703	526.40 ± 31.80
1908.3014 ± 0.1193	524.026237 ± 0.032768	0.2359 ± 0.0702	496.60 ± 46.44
1919.3508 ± 0.0539	521.009508 ± 0.014619	0.5170 ± 0.0701	455.07 ± 20.88
1921.9779 ± 0.0676	520.297335 ± 0.018295	0.4526 ± 0.0755	468.85 ± 25.53
1929.3992 ± 0.0100	518.296046 ± 0.002682	3.1239 ± 0.0755	402.29 ± 3.89
1930.8374 ± 0.0694	517.910003 ± 0.018616	0.4047 ± 0.0705	513.52 ± 26.76
1933.5527 ± 0.0076	517.182704 ± 0.002026	4.2646 ± 0.0778	259.92 ± 2.90
1934.2010 ± 0.0439	517.009347 ± 0.011739	0.6335 ± 0.0699	44.63 ± 16.89
1937.7357 ± 0.0054	516.066256 ± 0.001429	5.9070 ± 0.0751	430.56 ± 2.07
1940.6333 ± 0.0879	515.295703 ± 0.023332	0.3166 ± 0.0701	501.79 ± 33.64
1941.6345 ± 0.0526	515.029999 ± 0.013965	0.5783 ± 0.0742	512.29 ± 20.39
1945.3247 ± 0.0623	514.053010 ± 0.016466	0.4518 ± 0.0709	84.25 ± 23.85
1948.7083 ± 0.0780	513.160450 ± 0.020534	0.3801 ± 0.0720	117.80 ± 29.89
1953.2238 ± 0.0469	511.974107 ± 0.012304	0.5927 ± 0.0699	505.16 ± 17.87
1958.2977 ± 0.0757	510.647580 ± 0.019732	0.3779 ± 0.0707	106.62 ± 28.83
1960.5431 ± 0.0623	510.062738 ± 0.016211	0.4656 ± 0.0711	238.26 ± 23.85
1965.0174 ± 0.0716	508.901354 ± 0.018543	0.3990 ± 0.0712	91.53 ± 27.24
1970.0741 ± 0.0761	507.595116 ± 0.019606	0.3647 ± 0.0696	195.12 ± 28.70
2020.9997 ± 0.0385	494.804625 ± 0.009422	0.7243 ± 0.0700	431.68 ± 14.15
2025.1355 ± 0.0103	493.794131 ± 0.002508	2.7496 ± 0.0709	83.23 ± 3.77
2045.3755 ± 0.1085	488.907782 ± 0.025935	0.2561 ± 0.0697	288.79 ± 39.40
2206.1419 ± 0.0188	453.280005 ± 0.003857	1.5642 ± 0.0728	307.96 ± 6.29
2210.2752 ± 0.0107	452.432358 ± 0.002184	2.7965 ± 0.0740	339.80 ± 3.64

Table .16. continued.

Frequency (μHz)	Period (sec)	Amplitude (mma)	T_{max} (s)
2211.7581 ± 0.0757	452.129006 ± 0.015466	0.3696 ± 0.0701	156.57 ± 25.47
2214.3454 ± 0.0074	451.600738 ± 0.001513	3.9293 ± 0.0723	197.64 ± 2.51
2216.2287 ± 0.0570	451.216963 ± 0.011612	0.4867 ± 0.0698	134.57 ± 19.13
2226.2960 ± 0.0781	449.176562 ± 0.015747	0.3706 ± 0.0708	155.61 ± 26.10
2227.9061 ± 0.0578	448.851945 ± 0.011636	0.4996 ± 0.0709	178.28 ± 19.33
2239.4576 ± 0.0694	446.536693 ± 0.013838	0.3991 ± 0.0696	218.07 ± 23.03
2269.4107 ± 0.0224	440.643032 ± 0.004344	1.2648 ± 0.0703	115.71 ± 7.30
2276.7283 ± 0.0460	439.226755 ± 0.008873	0.6139 ± 0.0701	136.89 ± 14.92
2290.5488 ± 0.0389	436.576592 ± 0.007423	0.7237 ± 0.0704	247.51 ± 12.62
2339.1130 ± 0.0330	427.512477 ± 0.006032	0.8525 ± 0.0705	424.71 ± 10.48
2346.0971 ± 0.0353	426.239820 ± 0.006406	0.8032 ± 0.0706	195.92 ± 11.12
2359.4700 ± 0.0328	423.824003 ± 0.005897	0.8627 ± 0.0706	339.12 ± 10.29
2366.5109 ± 0.0154	422.563024 ± 0.002750	1.8229 ± 0.0704	117.34 ± 4.84
2380.0856 ± 0.0824	420.152952 ± 0.014551	0.3363 ± 0.0696	138.69 ± 25.73
2406.3307 ± 0.0235	415.570477 ± 0.004063	1.1894 ± 0.0701	114.34 ± 7.26
2413.0358 ± 0.0499	414.415741 ± 0.008570	0.5608 ± 0.0701	70.22 ± 15.35
2478.6019 ± 0.0322	403.453250 ± 0.005237	0.8725 ± 0.0703	401.63 ± 9.62
2485.4890 ± 0.0320	402.335323 ± 0.005185	0.8750 ± 0.0703	317.17 ± 9.56
2499.7528 ± 0.0355	400.039555 ± 0.005687	0.7880 ± 0.0705	151.33 ± 10.58
2559.0240 ± 0.0998	390.773989 ± 0.015244	0.2774 ± 0.0695	203.20 ± 28.99

Table .17. Detected pulsation modes in the 2002 dataset (T_{max} computed from T_o = 245 2410.0 BCT).

Frequency (μHz)	Period (sec)	Amplitude (mma)	T_{max} (s)
1070.6102 ± 0.0861	934.046767 ± 0.075104	0.5357 ± 0.0871	107.39 ± 50.77
1124.0253 ± 0.1287	889.659728 ± 0.101866	0.3526 ± 0.0859	688.36 ± 72.72
1139.3026 ± 0.0857	877.729971 ± 0.066030	0.5280 ± 0.0860	747.58 ± 47.88
1179.7990 ± 0.0944	847.601985 ± 0.067817	0.4948 ± 0.0887	765.09 ± 50.63
1224.8006 ± 0.1001	816.459446 ± 0.066728	0.4508 ± 0.0853	599.17 ± 51.69
1366.5982 ± 0.1319	731.743955 ± 0.070626	0.3443 ± 0.0860	74.59 ± 61.10
1371.3576 ± 0.1032	729.204412 ± 0.054864	0.5059 ± 0.0935	101.42 ± 44.89
1374.7202 ± 0.1422	727.420768 ± 0.075249	0.3224 ± 0.0867	487.34 ± 65.33
1375.5050 ± 0.0805	727.005714 ± 0.042522	0.5990 ± 0.0909	654.32 ± 36.96
1405.2834 ± 0.1118	711.600227 ± 0.056631	0.5233 ± 0.0949	417.45 ± 46.17
1412.9375 ± 0.1605	707.745398 ± 0.080389	0.2813 ± 0.0852	25.32 ± 71.73
1415.7909 ± 0.1342	706.318985 ± 0.066956	0.4019 ± 0.0911	501.06 ± 57.43
1435.0568 ± 0.1252	696.836548 ± 0.060794	0.3665 ± 0.0867	100.40 ± 55.05
1495.9336 ± 0.1321	668.478884 ± 0.059015	0.3456 ± 0.0853	55.45 ± 55.49
1514.0709 ± 0.1250	660.471055 ± 0.054510	0.3845 ± 0.0893	499.27 ± 50.25
1536.4736 ± 0.0983	650.841008 ± 0.041623	0.4947 ± 0.0891	540.22 ± 38.64
1596.2317 ± 0.1287	626.475476 ± 0.050510	0.3591 ± 0.0876	53.34 ± 50.99
1728.2481 ± 0.1071	578.620634 ± 0.035841	0.4318 ± 0.0868	375.10 ± 39.29
1780.0778 ± 0.0828	561.773192 ± 0.026133	0.5547 ± 0.0886	18.20 ± 29.57
1786.5244 ± 0.0824	559.746053 ± 0.025824	0.5639 ± 0.0871	434.82 ± 29.19
1790.7357 ± 0.0211	558.429697 ± 0.006571	2.2240 ± 0.0886	366.77 ± 7.44
1790.9382 ± 0.1458	558.366561 ± 0.045466	0.3097 ± 0.0851	366.77 ± 51.36
1794.0625 ± 0.0981	557.394184 ± 0.030472	0.4683 ± 0.0865	509.78 ± 34.56
1794.8864 ± 0.0447	557.138323 ± 0.013887	1.0415 ± 0.0878	315.93 ± 15.75
1809.4518 ± 0.0892	552.653564 ± 0.027232	0.5176 ± 0.0875	94.29 ± 31.06
1831.3343 ± 0.0487	546.049955 ± 0.014514	0.9362 ± 0.0861	536.28 ± 16.78
1836.2799 ± 0.0951	544.579286 ± 0.028195	0.4844 ± 0.0864	66.81 ± 32.62
1837.1193 ± 0.0794	544.330474 ± 0.023538	0.6341 ± 0.0963	125.39 ± 27.38
1846.8182 ± 0.0742	541.471815 ± 0.021759	0.6357 ± 0.0904	88.89 ± 24.95
1848.8445 ± 0.2050	540.878378 ± 0.059977	0.2298 ± 0.0869	283.10 ± 69.56
1853.6162 ± 0.0910	539.486009 ± 0.026483	0.5071 ± 0.0872	154.66 ± 31.02
1854.0242 ± 0.0060	539.367285 ± 0.001760	8.3568 ± 0.0943	430.10 ± 2.05
1858.1503 ± 0.0161	538.169592 ± 0.004669	2.9824 ± 0.0910	199.88 ± 5.48
1861.8588 ± 0.0845	537.097655 ± 0.024364	0.5706 ± 0.0946	142.98 ± 28.37
1862.1695 ± 0.0440	537.008057 ± 0.012676	1.1613 ± 0.0958	78.57 ± 14.79
1880.2493 ± 0.0451	531.844376 ± 0.012771	1.0293 ± 0.0867	405.53 ± 15.23
1881.1465 ± 0.0896	531.590703 ± 0.025327	0.5358 ± 0.0916	171.05 ± 29.55
1896.0151 ± 0.0791	527.421973 ± 0.022008	0.6424 ± 0.0973	117.94 ± 25.63
1899.5102 ± 0.0596	526.451492 ± 0.016518	0.7695 ± 0.0866	445.05 ± 19.82
1924.3662 ± 0.0694	519.651606 ± 0.018740	0.7102 ± 0.0903	197.67 ± 23.19
1925.7273 ± 0.1793	519.284327 ± 0.048361	0.2580 ± 0.0864	186.83 ± 58.67
1925.7573 ± 0.0850	519.276242 ± 0.022910	0.5794 ± 0.0905	174.21 ± 28.38
1926.9414 ± 0.1290	518.957139 ± 0.034731	0.3572 ± 0.0863	49.20 ± 42.41
1928.1807 ± 0.1029	518.623600 ± 0.027670	0.4430 ± 0.0862	328.53 ± 33.71
1929.3921 ± 0.0287	518.297980 ± 0.007708	1.7091 ± 0.0921	100.33 ± 9.27
1933.6410 ± 0.0191	517.159088 ± 0.005107	2.4516 ± 0.0887	198.49 ± 6.24
1937.1805 ± 0.0951	516.214164 ± 0.025330	0.4936 ± 0.0879	27.52 ± 30.81
1937.5984 ± 0.0070	516.102831 ± 0.001862	7.2537 ± 0.0946	434.69 ± 2.28
1941.9776 ± 0.0730	514.938987 ± 0.019356	0.6935 ± 0.0946	137.30 ± 23.83
1942.7075 ± 0.0851	514.745523 ± 0.022550	0.5492 ± 0.0881	139.88 ± 27.53
2008.9093 ± 0.0996	497.782543 ± 0.024687	0.4577 ± 0.0863	32.45 ± 31.29
2136.8990 ± 0.1556	467.967828 ± 0.034076	0.2920 ± 0.0860	270.93 ± 46.03
2170.5511 ± 0.1300	460.712495 ± 0.027588	0.3551 ± 0.0890	83.61 ± 38.07
2172.6801 ± 0.2086	460.261035 ± 0.044183	0.2266 ± 0.0867	188.87 ± 60.42
2195.1020 ± 0.1247	455.559702 ± 0.025882	0.3727 ± 0.0895	230.03 ± 36.05
2198.5986 ± 0.1632	454.835188 ± 0.033755	0.3698 ± 0.1013	219.14 ± 41.48
2199.7496 ± 0.1770	454.597206 ± 0.036576	0.3172 ± 0.0900	151.45 ± 50.00
2203.3154 ± 0.0909	453.861480 ± 0.018723	0.6159 ± 0.0987	211.71 ± 25.04
2206.1699 ± 0.0319	453.274258 ± 0.006552	1.4671 ± 0.0886	243.59 ± 9.15
2208.6948 ± 0.1069	452.756075 ± 0.021920	0.4326 ± 0.0876	280.92 ± 30.53
2209.8242 ± 0.1304	452.524684 ± 0.026693	0.4560 ± 0.1021	204.12 ± 33.23
2210.2000 ± 0.0173	452.447752 ± 0.003544	2.7767 ± 0.0911	75.01 ± 4.95
2212.4681 ± 0.1416	451.983909 ± 0.028921	0.3813 ± 0.0901	422.65 ± 40.78
2214.4441 ± 0.0146	451.580605 ± 0.002985	3.3943 ± 0.0941	171.35 ± 4.18
2215.3478 ± 0.1491	451.396388 ± 0.030380	0.3748 ± 0.0987	328.11 ± 40.86
2224.9708 ± 0.1838	449.444093 ± 0.037129	0.2551 ± 0.0880	227.54 ± 51.97
2232.6552 ± 0.1923	447.897205 ± 0.038583	0.2390 ± 0.0869	317.15 ± 54.29
2270.2367 ± 0.0637	440.482714 ± 0.012354	0.7243 ± 0.0872	50.70 ± 17.74
2276.6719 ± 0.0774	439.237640 ± 0.014935	0.5979 ± 0.0876	254.15 ± 21.51
2290.7585 ± 0.1186	436.536633 ± 0.022598	0.3902 ± 0.0876	42.62 ± 32.67
2303.3819 ± 0.0951	434.144256 ± 0.017933	0.4816 ± 0.0866	142.89 ± 26.22
2312.8515 ± 0.1140	432.366722 ± 0.021303	0.4549 ± 0.0872	87.10 ± 29.16
2323.5281 ± 0.2197	430.379995 ± 0.040693	0.2365 ± 0.0863	238.33 ± 56.16
2338.6337 ± 0.0376	427.600100 ± 0.006869	1.3643 ± 0.0940	150.88 ± 10.07
2339.5492 ± 0.2815	427.432772 ± 0.051422	0.1616 ± 0.0861	260.01 ± 76.26
2344.2511 ± 0.1114	426.575472 ± 0.020270	0.4168 ± 0.0878	163.77 ± 30.01
2345.7248 ± 0.0492	426.307468 ± 0.008938	0.9784 ± 0.0909	327.08 ± 13.27
2358.0435 ± 0.0825	424.080388 ± 0.014837	0.5594 ± 0.0872	316.62 ± 22.14
2366.4338 ± 0.0313	422.576783 ± 0.005580	1.6362 ± 0.0941	105.47 ± 8.29
2376.0473 ± 0.1284	420.867035 ± 0.022749	0.3506 ± 0.0855	245.65 ± 34.21
2405.2427 ± 0.0894	415.758461 ± 0.015461	0.5093 ± 0.0860	105.21 ± 23.51
2413.5025 ± 0.0662	414.335592 ± 0.011373	0.6977 ± 0.0871	130.27 ± 17.33
2418.2414 ± 0.0802	413.523652 ± 0.013719	0.5829 ± 0.0887	228.47 ± 20.99

Table .17. continued.

Frequency (μHz)	Period (sec)	Amplitude (mma)	T_{max} (s)
2426.9190 ± 0.0718	412.045069 ± 0.012195	0.6427 ± 0.0876	61.36 ± 18.76
2454.1297 ± 0.1375	407.476435 ± 0.022832	0.3532 ± 0.0881	52.49 ± 36.61
2466.5843 ± 0.1430	405.418952 ± 0.023503	0.3630 ± 0.0930	308.39 ± 36.59
2477.0475 ± 0.0917	403.706433 ± 0.014943	0.5014 ± 0.0871	395.12 ± 23.41
2493.0801 ± 0.1250	401.110256 ± 0.020111	0.3771 ± 0.0896	275.03 ± 31.96
2494.2523 ± 0.1651	400.921744 ± 0.026537	0.2889 ± 0.0877	253.69 ± 41.98
2499.7609 ± 0.0753	400.038258 ± 0.012052	0.6148 ± 0.0875	213.83 ± 19.05
2505.3706 ± 0.0700	399.142542 ± 0.011157	0.6596 ± 0.0870	67.48 ± 17.59
2517.2488 ± 0.1433	397.259101 ± 0.022617	0.3349 ± 0.0902	226.23 ± 36.19
2518.7564 ± 0.1643	397.021324 ± 0.025902	0.2769 ± 0.0860	294.01 ± 41.27
2527.2090 ± 0.1941	395.693427 ± 0.030384	0.2460 ± 0.0872	329.32 ± 47.98
2547.8652 ± 0.1658	392.485442 ± 0.025543	0.2790 ± 0.0877	79.07 ± 41.68
2557.9851 ± 0.3118	390.932688 ± 0.047647	0.1483 ± 0.0877	232.22 ± 77.72
2561.8125 ± 0.2072	390.348636 ± 0.031567	0.2224 ± 0.0872	49.50 ± 51.04
2580.7262 ± 0.1065	387.487827 ± 0.015996	0.4336 ± 0.0871	61.83 ± 26.00
2642.6779 ± 0.1131	378.404050 ± 0.016191	0.4069 ± 0.0871	212.25 ± 27.04
2647.3574 ± 0.0767	377.735169 ± 0.010950	0.6011 ± 0.0871	225.95 ± 18.32
2675.6539 ± 0.0842	373.740420 ± 0.011765	0.5884 ± 0.0939	161.95 ± 19.92
2799.7842 ± 0.1911	357.170391 ± 0.024379	0.2453 ± 0.0885	87.83 ± 43.21
2829.5995 ± 0.1772	353.406907 ± 0.022129	0.2588 ± 0.0868	74.56 ± 39.59
2881.6572 ± 0.1588	347.022543 ± 0.019122	0.2872 ± 0.0864	244.89 ± 34.85
3560.1456 ± 0.1034	280.887389 ± 0.008155	0.4369 ± 0.0857	96.01 ± 18.38

List of Objects